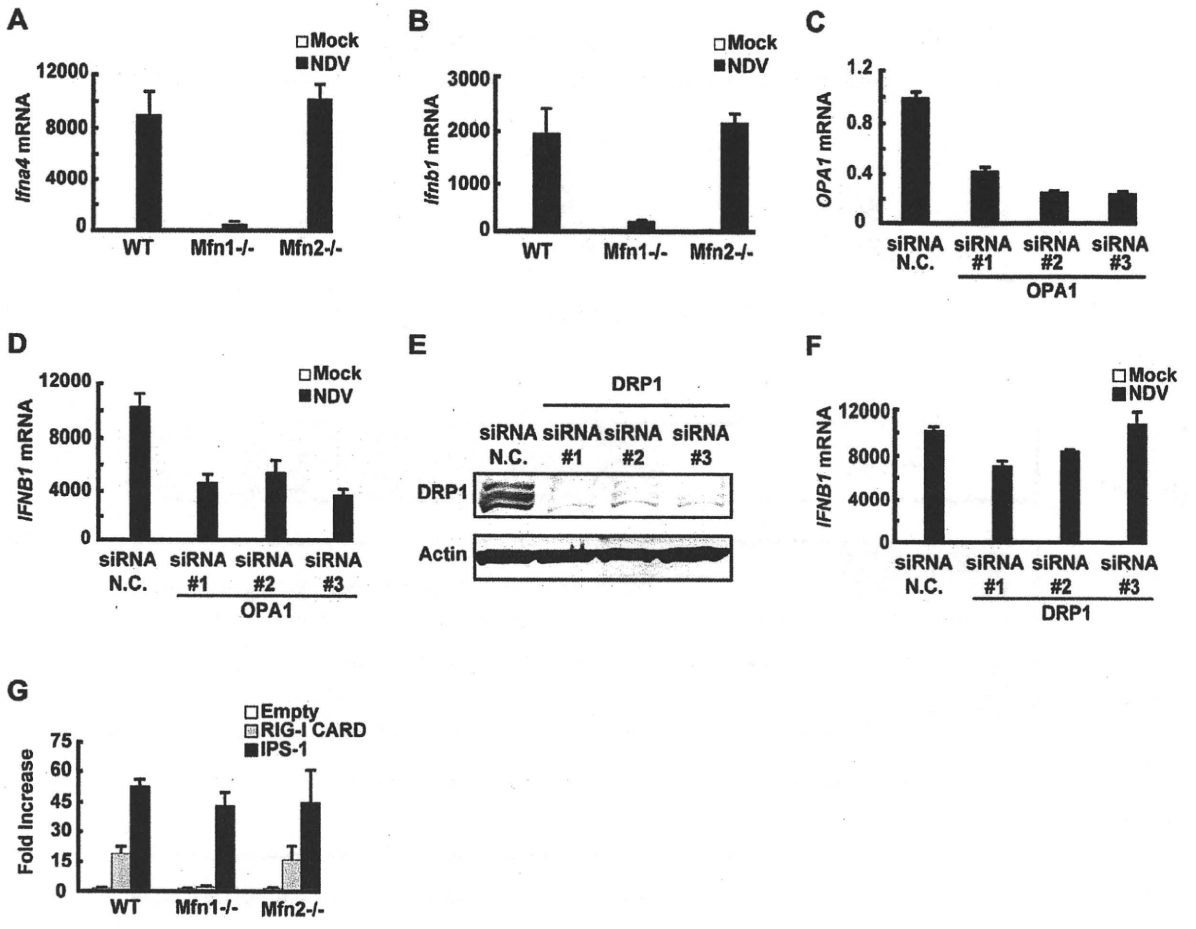

Figure 9. MFN1 plays a critical role in RIG-I–induced signaling. A and **B**, Wild-type (WT) MEFs and Mfn1 or Mfn2-knockout MEFs were infected with NDV for 9 h. The levels of endogenous *Ifna4* (**A**) and *Ifnb1* (**B**) mRNA were quantified by qRT-PCR. **C**, HeLa cells were transfected with negative control (N.C.) or hOPA1-targeted siRNA (#1–#3) for 72 h, and the expression of *OPA1* mRNA was analyzed by qRT-PCR. **D**, HeLa cells were transfected with N.C. siRNA or hOPA1-targeted siRNA. 72 h after transfection, cells were infected with NDV for 12 h. *IFNB1* mRNA expression was quantified by qRT-PCR. **E**, HeLa cells were transfected with N.C. siRNA or hDRP1-targeted siRNA (#1–#3) for 72 h, and the knockdown of endogenous DRP1 was analyzed by Western blotting using anti-DRP1 antibody. **F**, HeLa cells were transfected with N.C. siRNA or hDRP1-targeted siRNA. At 72 h after transfection, cells were infected with NDV for 12 h. *IFNB1* mRNA expression was quantified by qRT-PCR. **G**, WT and Mfn1 or Mfn2-knockout MEFs were transfected with a virus-responsive reporter gene (p-125 Luc) with either an empty vector (Empty) or an expression vector for RIG-I CARD or IPS-1. Luciferase activity was determined 48 h after transfection. Data represent means ± s.d. (n=3).
doi:10.1371/journal.ppat.1001012.g009

mitochondria and finally accumulates densely on others. On the other hand, forced overexpression of full-length IPS-1 results in constitutive signaling [7,8,9,10]. There is no clear explanation why non-physiological overexpression can by-pass the virus-induced signaling, however, it can be concluded that transient IPS-1 overexpression may quantitatively override the hypothetical inhibitor for IPS-1 (above). Under these conditions, MFN1 is dispensable (Fig. 9G). Consistent with this, artificial aggregation of IPS-1 by cross-linking induced the signaling to activate IFN genes (Tang, E. D. and Wang, C. D. [24] and our unpublished observation). We speculate that under physiological conditions, viral infection induces the local accumulation of IPS-1 (corresponds to "active IPS-1") on mitochondria. These mitochondria with locally accumulated IPS-1 may function as a platform to recruit downstream molecules.

MFN1 and MFN2 are structurally similar and both occur on the outer membrane of mitochondria. Their functions however are not redundant, as the single knockout of either produces a certain mitochondrial phenotype [19]. Recently two papers were published concerning MFN function in RIG-I-mediated antiviral responses. Yasukawa et al. reported that MFN2 strongly interacts with IPS-1 thereby blocking its function, however MFN1 does not interact with IPS-1 and exhibits no effect [25]. These observations are clearly inconsistent with ours. The report by Castanier et al. however, is consistent with our finding that MFN1, but not MFN2, positively regulates IPS-1 [26]. Most importantly, our knockout results are clearly consistent with their knockdown results (Fig. 9A and B). Castanier et al. observed that a particular variant of SeV (H4) causes elongation of mitochondria, however they did not demonstrate whether this morphological change is common to other viral infections. Unlike Castanier et al. we did not observe mitochondrial elongation by viral infections nor 5′-pppRNA transfection (Fig. 3). The knockdown of a mitochondrial inner membrane protein OPA1 blocked virus-induced signaling

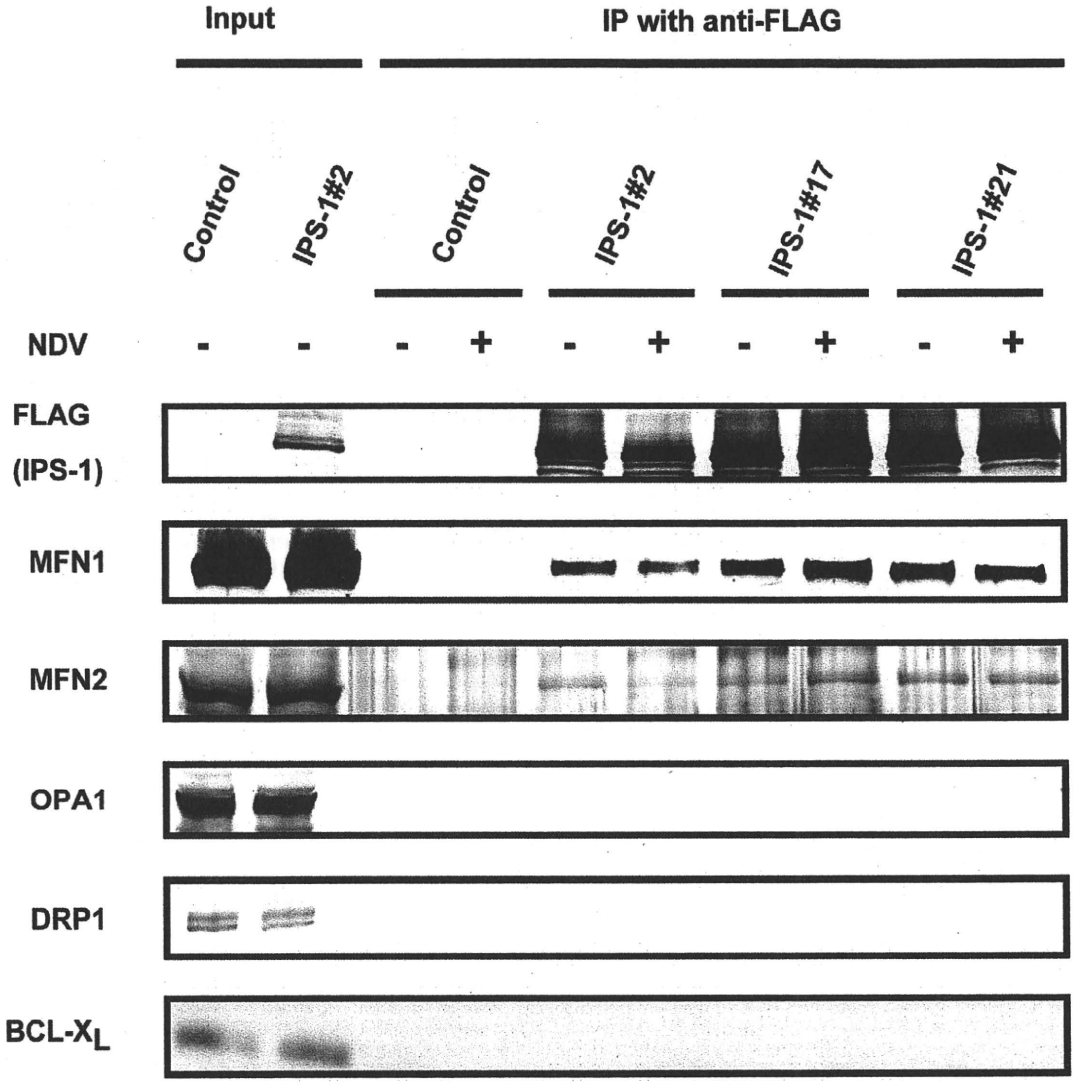

Figure 10. IPS-1 interacts with MFN1 and MFN2. IPS-1-HeLa cells were infected with NDV for 12 h, and then FLAG-IPS-1 was immunoprecipitated with anti-FLAG antibody. Co-immunoprecipitated MFN1 and MFN2 were detected by anti-MFN1 antibody and anti-MFN2 antibody, respectively. Neither OPA1 nor DRP1 was co-immunoprecipitated with FLAG-IPS-1. Mitochondrial protein BCL-XL was used as a control and was also examined by anti-BCLXL antibody.
doi:10.1371/journal.ppat.1001012.g010

(Fig. 9D); thereby indicating that mitochondrial fusion may be necessary for the activation of IPS-1. Castanier et al. observed that knockdown of DRP1 or FIS1 causes mitochondrial elongation and IPS-1's association with STING, an antiviral signaling adaptor. However, neither the mitochondrial elongation nor the IPS-1-STING interaction is sufficient to activate the signaling.

We demonstrated that the redistribution of IPS-1 is induced by various viral infections and 5′ppp-RNA transfection and is dependent on a functional MFN1. The precise mechanism of the IPS-1 redistribution is not known, however we propose a model described in Fig. 13. In uninfected cells, MFN1 and IPS-1 associate constitutively (Fig. 10) and distribute evenly on all mitochondria. When a virus replicates in a specific cytoplasmic compartment, RIG-I is recruited to this area as a result of interaction with viral dsRNA through the C-terminal RNA-binding domain (Fig. 5A). Upon binding with viral RNA, CARD is exposed (activate RIG-I) [27], and then interacts with IPS-1 at the periphery of the viral compartment. At the same time, mitochondria surround the viral compartment because it lacks the ability to penetrate it (Fig. 6). Since mitochondrion is an elastic, movable organelle [28], affinity between RIG-I and IPS-1 may be sufficient for the mitochondrial relocalization. IPS-1/MFN1 complex may facilitate fusion between the surrounding mitochondria. Mitochondrial fission occurs independently to balance the fusion, however since the fusion of IPS-1/MFN1-enriched mitochondria facilitates the redistribution of IPS-1, IPS-1-enriched mitochondria may be generated. Further research is necessary to elucidate if the mitochondrial fusion process is indeed central to IPS-1 redistribution.

In summary, our study provides new insight into why the mitochondrial localization of IPS-1 is essential to its function. We

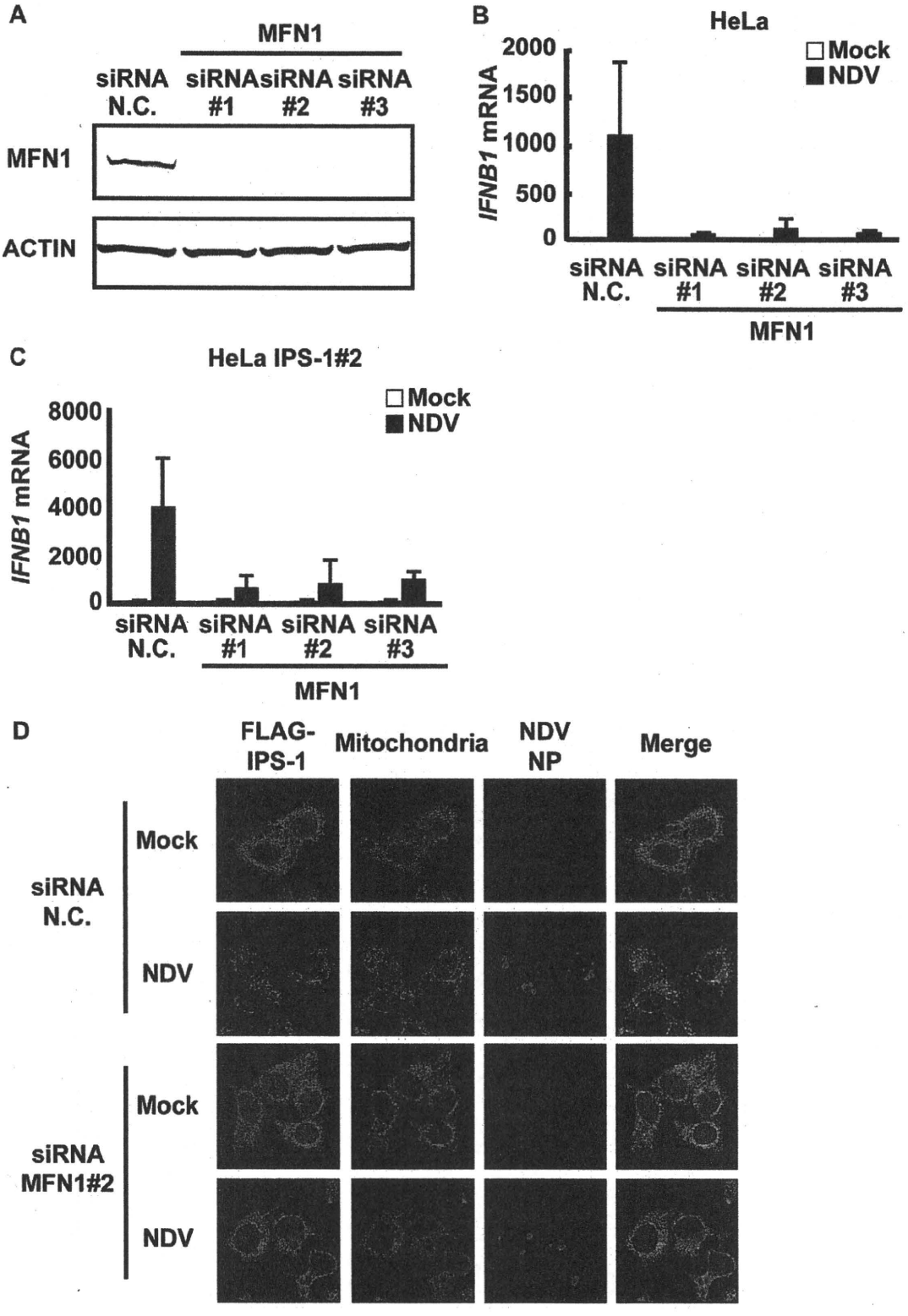

Figure 11. Knockdown of MFN1 inhibits the redistribution of IPS-1 induced by NDV infection. A, HeLa cells were transfected with negative control (N.C.) or hMFN1-targeted siRNA (#1–#3) for 48 h, and the knockdown of endogenous MFN1 was analyzed by Western blotting using anti-MFN1 antibody. **B**, Cells transfected with siRNA as shown in **a** were infected with NDV for 12 h, and endogenous *IFNB1* mRNA expression

was quantified by qRT-PCR. Data represent means ± s.d. (n = 3). **C**, IPS-1-HeLa cells transfected with N.C. or hMFN1-targeted siRNA were infected with NDV for 12 h, and endogenous *IFNB1* mRNA expression was quantified by qRT-PCR. Data represent means ± s.d. (n = 3). **D**, IPS-1-HeLa cells transfected with N.C. or hMFN1-targeted siRNA#2 for 48 h. Cells were infected with NDV for 12 h and stained with anti-FLAG antibody (FLAG-IPS-1), anti-NP antibody (NDV NP), and MitoTracker (Mitochondria).
doi:10.1371/journal.ppat.1001012.g011

demonstrated that MFN1 regulates the redistribution of IPS-1 in a RIG-I-signal-dependent manner. The mitochondrion provides a platform for the coordination of antiviral signaling by receiving the initial signal from the activated RIG-I. The signal is amplified through the accumulation of IPS-1, and other essential molecules such as tumor necrosis factor receptor-associated factors (TRAFs) and signaling protein kinases are recruited to mobilize active transcriptional regulators. In this regard, another organelle, the late endosome, functions similarly as a platform for antiviral signaling by recruiting different signaling components. This is initiated by Toll-like receptors (TLR3, 7, 8, and 9), another subtype of nucleic acid sensors.

Materials and Methods

Cell culture and transfection

HeLa, SKHep1, MEF, and 293T cells were maintained in Dulbecco's modified Eagle's medium with 10% fetal bovine serum and penicillin–streptomycin (100U/ml and 100μg/ml, respectively). L929 cells were maintained in minimum essential medium with 5% fetal bovine serum and penicillin-streptomycin. Immortalized wild-type MEFs and MEFs deficient in Mfn1 or Mfn2 were obtained from Prof. David Chan (Caltech). HeLa, L929, and 293T cells were transfected with Lipofectamine 2000 (Invitrogen). Stable transformants of IPS-1-HeLa cells were established by transfection of a linearized empty plasmid (pEF-Tak) or expression plasmid for FLAG-IPS-1 (pEF-Tak-FLAG-IPS-1), and selected with G418 (1mg/ml). We used HeLa IPS-1#2 clone for most experiments because IPS-1#2 clone showed higher induction of IFN among the stable clones, but we confirmed that other clones also showed the same phenotype. IPS-1/RIG-Iwt and IPS-1/RIG-I K270A-expressing HeLa cells were generated by transduction using a lentivirus system. cDNA for RIG-I wt or RIG-I K270A was cloned into the multi-cloning site of a lentiviral vector, pCSII-CMV-MCS-IRES2-Bsd. The recombinant lentiviruses were generated by co-transfection of the lentiviral vector together with lentivirus constructs, pCMV-VSV-G-RSV-Rev and pCAG-HIVgp, into 293T cells. At 48 h post-transfection, the culture supernatant was collected, and then added to IPS-1#2 HeLa cells. Three days later, the cells were selected with Blasticidin (10μg/ml).

Viral infection and plaque assay

Cells were treated with culture medium or infected with SeV, NDV, Sindbis virus, EMCV, Influenza virus, or VSV at a MOI of 1 or 0.5 for qRT-PCR or immunofluorescence, respectively. The

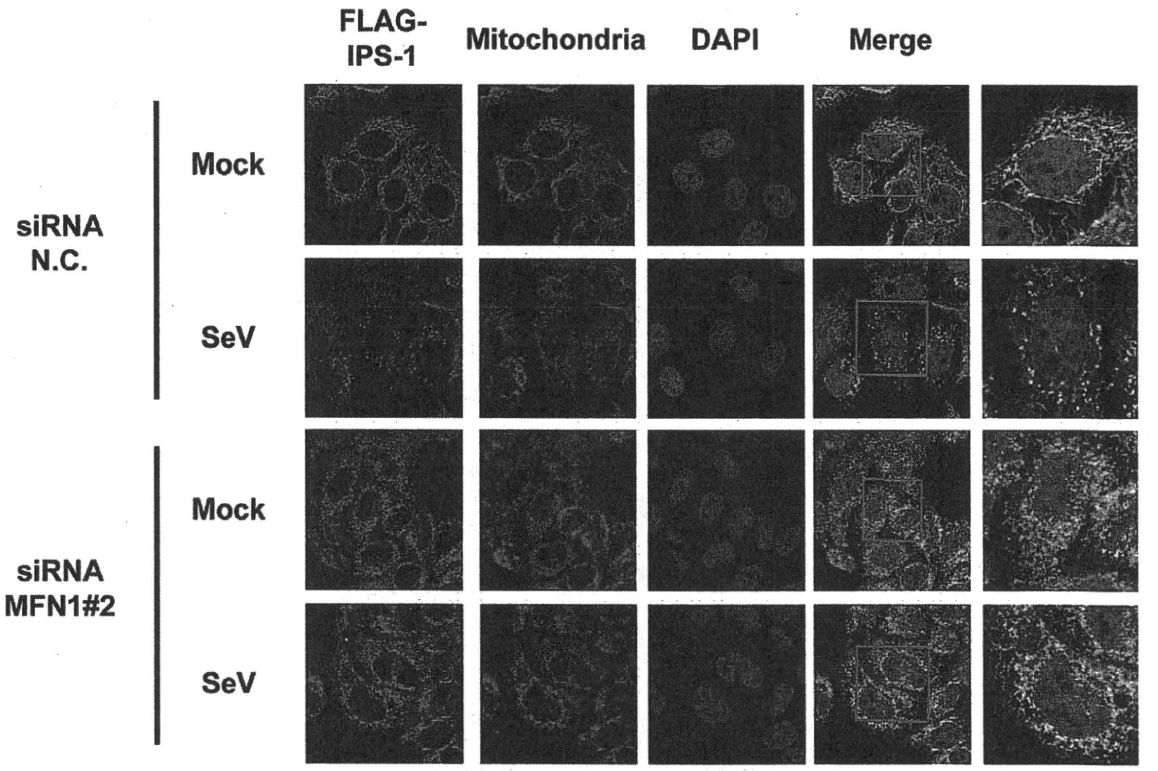

Figure 12. Knockdown of MFN1 inhibits the redistribution of IPS-1 induced by SeV infection. IPS-1-HeLa cells transfected with negative control (N.C.) or hMFN1-targeted siRNA#2 for 48 h. Cells were infected with SeV for 12 h and stained with anti-FLAG antibody (FLAG-IPS-1), MitoTracker (Mitochondria), and DAPI. The area enclosed by the red rectangle is enlarged at the right.
doi:10.1371/journal.ppat.1001012.g012

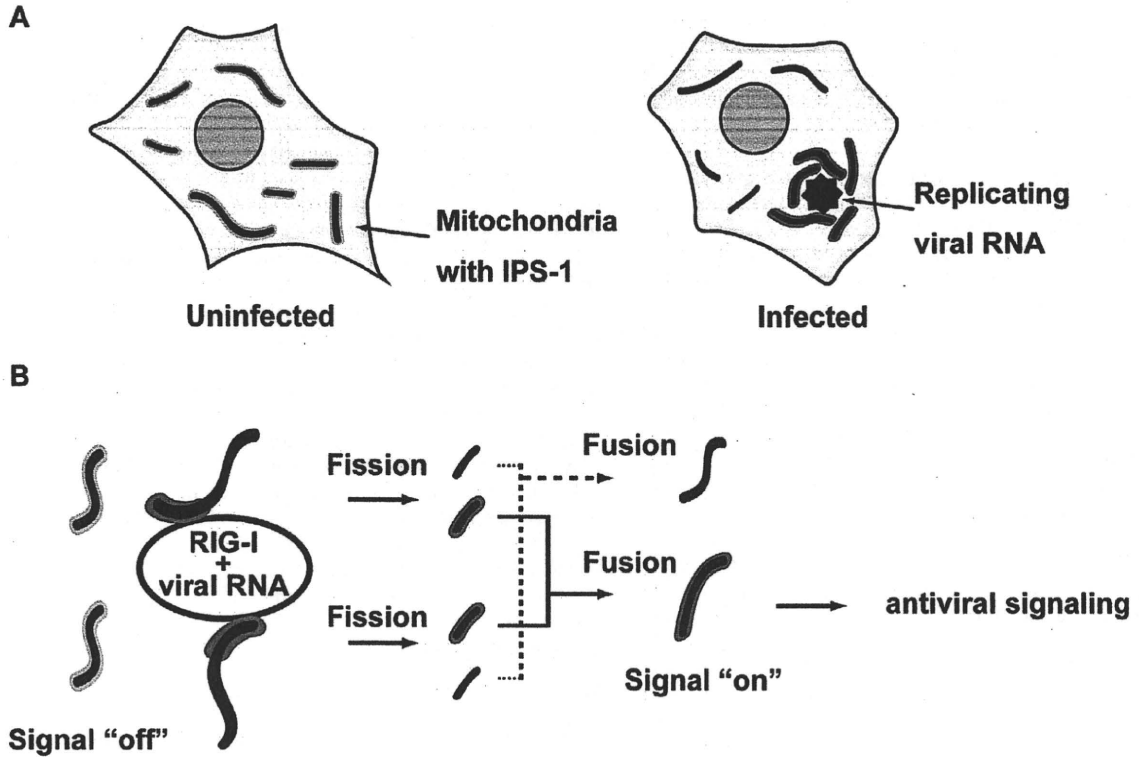

Figure 13. Model for the redistribution of IPS-1 mediated by mitochondrial organization. A, Schematic representation of the redistribution of IPS-1 induced by viral infection. In uninfected cells, IPS-1 is evenly distributed in all mitochondria (left). In infected cells, foci of viral nucleoprotein form, which are surrounded by redistributed IPS-1 and mitochondria (right). **B**, A model for the redistribution of IPS-1 mediated by mitochondrial organization. Initially, IPS-1 is distributed evenly in mitochondria (left). Viruses replicate in restricted compartments in the cells, viral RNA accumulates, and then RIG-I re-localizes to these compartments. Viral RNA induces a conformational change of RIG-I, and results in mitochondria expressing accumulated IPS-1- around the RIG-I foci. IPS-1 may be redistributed, resulting in a local accumulation of IPS-1 on a mitochondrion (left). IPS-I may further segregate due to mitochondrial reorganization by fusion and fission (right). Local accumulation of IPS-1 may further recruit adaptors and protein kinases to activate antiviral signaling.
doi:10.1371/journal.ppat.1001012.g013

yield of EMCV in the culture supernatant was determined with a standard plaque assay [17].

Plasmid constructs

pEF-Bos-FLAG-RIG-I CARD and pEF-Bos-FLAG-IPS-1 have been described previously [6,17]. pEF-Tak and pEF-Tak-FLAG-IPS-1 were kindly provided by Dr. M. Gale (University of Washington School of Medicine, USA). pEF-Bos-HA-MFN1 and pEF-Bos-HA-MFN2 were newly constructed. MFN1 and MFN2 cDNA were amplified with a pair of oligonucleotides designed to add an N-terminal HA tag by PCR, and the PCR fragment was inserted into pEF-Bos(+). MFN2 cDNA was purchased from the Biological Resource Center of the National Institute of Technology and Evaluation of Japan. pEF-Bos-HA-MFN1 T109A was constructed with a KOD-Plus-Mutagenesis kit (TOYOBO, Japan). The nucleotide sequences for the constructs were confirmed with the BigDye DNA sequencing kit (Applied Biosystems). Luciferase reporter containing human IFN-β promoter/enhancer (−125-Luc) is described elsewhere [29].

Synthetic RNA

Nucleotide sequences of the synthetic RNA were described previously [14]. 5′ppp-RNA was synthesized by in vitro transcription using the T7 Megascript kit (Ambion). 5′OH-RNA was chemically synthesized (Japan Bio Services Co., Ltd, Japan) and synthetic RNA was transfected by Lipofectamine RNAiMax (20 pmol in a 24-well format).

Immunoblotting, luciferase assay, and antibodies

The preparation of cell extracts, luciferase assay, and immunoblotting have already been described [17,29]. The antibodies used are: anti-FLAG antibody (SIGMA: F3165 and Affinity Bioreagents: PA1-984B), anti-ERAB antibody (Abcam: ab10260), anti-MFN1 antibody (Santa cruiz: sc-50330), anti-ACTIN antibody (Millipore: MAB150 1R), anti-MFN2 antibody (abcam: ab56889), anti-OPA1 antibody (abcam: ab42364), anti-DRP1 antibody (abcam: ab56788), and anti-BCLXL (Santa cruiz: sc-8392). The anti-NP antibody was produced by Dr. Y. Nagai, and provided by Dr. T. Sakaguchi (Hiroshima University, Japan). The anti-RIG-I antibody was generated by immunizing a rabbit with a synthetic peptide corresponding to a.a. 793–807 of RIG-I. The generation of the anti-IPS-1 guinea pig antibody has already been described [30]. Briefly, anti-IPS-1 rabbit antibody was generated by immunizing a rabbit with a recombinant protein corresponding to a.a. 1–157 of IPS-1.

RNAi

The siRNA negative control and siRNAs targeting MFN1, OPA1, or DRP1 were purchased from Invitrogen, and transfected

with RNAi MAX (Invitrogen) according to the manufacturer's recommendation (final concentration of siRNA was 50nM). At 48 or 72 h post-transfection, cells were harvested or infected with NDV or SeV, then subjected to qRT-PCR, immunofluorescence, or SDS-PAGE followed by immunoblotting.

Quantitative real time PCR and microarray analysis

Total RNA was prepared with TRIZOL (Invitrogen) and treated with DNase I (Roche Diagnostics). A High-Capacity cDNA Reverse Transcription Kit (Applied Biosystems) was used for cDNA synthesis, and mRNA level was monitored with the Step One plus Real Time PCR system and TaqMan Fast Universal PCR Master Mix (Applied Biosystems). TaqMan primer-probes for human *IFNB1*, human *OPA1*, murine *Ifna4*, murine *Ifnb1*, and 18s rRNA were purchased from Applied Biosystems. The RNA copy numbers were normalized to that of internal 18s rRNA. In the microarray analysis, we used the Genopal microarray system according to the manufacturer's instructions (Mitsubishi Rayon). Biotin-labeled RNA was prepared with a MessageAmp II-Biotin Enhanced kit (Ambion).

Immunofluorescence and immunoelectron microscopy

For immunofluorescence analysis, cells were fixed with 4% paraformaldehyde for 10 min, permeabilized with an acetone: methanol (1:1) solution, and blocked with 5mg/ml of BSA in PBST (PBS, 0.04% Tween20) for 1 hour. The cells were next incubated with relevant primary antibodies overnight at 4°C, and then incubated with relevant Alexa Fluor 405, Alexa Fluor 488, or Alexa Fluor 594-conjugated secondary antibodies. Mitochondria were stained with MitoTracker Red CMXRos according to the manufacturer's instructions (Molecular Probes). Nuclei were stained with DAPI (4.6-diamidino-2-phenylinodole). The fluorescence image was quantified by software provided by Leica Microsystems. The percentage of IPS-1 redistribution among NDV-infected cells was scored by 3 persons, and data are shown as means ± s.d. of the three independent scores. Cells were analyzed with a Leica confocal laser-scanning microscope (TCS-SP2). For immunoelectron microscopy, cells were fixed with 4% paraformaldehyde and 0.05% and 0.01% glutaraldehyde for 10 min to detect NP and the FLAG tag, respectively, and then incubated with PBS containing 20% normal goat serum (NGS) and 0.075% Photo-Flo (Kodak) for 30 min at room temperature. The cells were incubated with the anti-NDV NP antibody or anti-FLAG antibody in PBS containing 2% NGS and 0.075% Photo-Flo overnight. After several washes with PBS, the cells were further incubated with a 1.4 nm gold-conjugated anti-mouse IgG goat IgG Fab fragment (Nanoprobes) in PBS containing 2% NGS and 0.075% Photo-Flo overnight. They were then washed with PBS and postfixed with 0.1 M phosphate buffer containing 1% (v/v) glutaraldehyde for 10 min at room temperature. After washing in distilled water, the gold particles were silver-intensified with an HQ silver kit (Nanoprobes) for 10–15 min. Then, the immunostained cells were incubated with 0.5% osmium tetroxide in 0.1M phosphate buffer for 40 min at room temperature. After dehydration with ethanol, cells were embedded in epoxy resin (Luveak 812; Nacalai Tesque, Japan). Once the resin was polymerized, the cells were cut into ultrathin sections on an ultramicrotome, Reichert-Nissei Ultracut S (Leica). The ultrathin sections were mounted on mesh grids, and stained by the Reynolds method. Finally, the ultrathin sections were examined with an electron microscope (H-7650; Hitachi).

Acknowledgments

We thank K. Furuta and H. Kohda for helping with the electron microscopy, T. Sakaguchi for the anti-NP antibody, M. Gale for the plasmid constructs, H. Miyoshi for the lentiviral vectors, and Mitsubishi Rayon for the microarray chip.

Author Contributions

Conceived and designed the experiments: K. Onoguchi, M. Yoneyama, T. Fujita. Performed the experiments: K. Onoguchi, K. Onomoto, S. Takamatsu, M. Jogi, A. Takemura, S. Morimoto. Analyzed the data: K. Onoguchi, H. Namiki, M. Yoneyama, T. Fujita. Contributed reagents/materials/analysis tools: I. Julkunen. Wrote the paper: K. Onoguchi, M. Yoneyama, T. Fujita.

References

1. Samuel CE (2001) Antiviral actions of interferons. Clin Microbiol Rev 14: 778–809, table of contents.
2. Theofilopoulos AN, Baccala R, Beutler B, Kono DH (2005) Type I interferons (alpha/beta) in immunity and autoimmunity. Annu Rev Immunol 23: 307–336.
3. Kotenko SV, Gallagher G, Baurin VV, Lewis-Antes A, Shen M, et al. (2003) IFN-lambdas mediate antiviral protection through a distinct class II cytokine receptor complex. Nat Immunol 4: 69–77.
4. Sheppard P, Kindsvogel W, Xu W, Henderson K, Schlutsmeyer S, et al. (2003) IL-28, IL-29 and their class II cytokine receptor IL-28R. Nat Immunol 4: 63–68.
5. Yoneyama M, Fujita T (2009) RNA recognition and signal transduction by RIG-I-like receptors. Immunol Rev 227: 54–65.
6. Onoguchi K, Yoneyama M, Takemura A, Akira S, Taniguchi T, et al. (2007) Viral infections activate types I and III interferon genes through a common mechanism. J Biol Chem 282: 7576–7581.
7. Kawai T, Takahashi K, Sato S, Coban C, Kumar H, et al. (2005) IPS-1, an adaptor triggering RIG-I- and Mda5-mediated type I interferon induction. Nat Immunol 6: 981–988.
8. Meylan E, Curran J, Hofmann K, Moradpour D, Binder M, et al. (2005) Cardif is an adaptor protein in the RIG-I antiviral pathway and is targeted by hepatitis C virus. Nature 437: 1167–1172.
9. Seth RB, Sun L, Ea CK, Chen ZJ (2005) Identification and characterization of MAVS, a mitochondrial antiviral signaling protein that activates NF-kappaB and IRF 3. Cell 122: 669–682.
10. Xu LG, Wang YY, Han KJ, Li LY, Zhai Z, et al. (2005) VISA is an adapter protein required for virus-triggered IFN-beta signaling. Mol Cell 19: 727–740.
11. Arnoult D, Carneiro L, Tattoli I, Girardin SE (2009) The role of mitochondria in cellular defense against microbial infection. Semin Immunol 21: 223–232.
12. Hornung V, Ellegast J, Kim S, Brzozka K, Jung A, et al. (2006) 5'-Triphosphate RNA is the ligand for RIG-I. Science 314: 994–997.
13. Pichlmair A, Schulz O, Tan CP, Naslund TI, Liljestrom P, et al. (2006) RIG-I-mediated antiviral responses to single-stranded RNA bearing 5'-phosphates. Science 314: 997–1001.
14. Takahasi K, Yoneyama M, Nishihori T, Hirai R, Kumeta H, et al. (2008) Nonself RNA-sensing mechanism of RIG-I helicase and activation of antiviral immune responses. Mol Cell 29: 428–440.
15. Benard G, Karbowski M (2009) Mitochondrial fusion and division: Regulation and role in cell viability. Semin Cell Dev Biol 20: 365–374.
16. Iwamura T, Yoneyama M, Koizumi N, Okabe Y, Namiki H, et al. (2001) PACT, a double-stranded RNA binding protein acts as a positive regulator for type I interferon gene induced by Newcastle disease virus. Biochem Biophys Res Commun 282: 515–523.
17. Yoneyama M, Kikuchi M, Natsukawa T, Shinobu N, Imaizumi T, et al. (2004) The RNA helicase RIG-I has an essential function in double-stranded RNA-induced innate antiviral responses. Nat Immunol 5: 730–737.
18. Santel A, Frank S, Gaume B, Herrler M, Youle RJ, et al. (2003) Mitofusin-1 protein is a generally expressed mediator of mitochondrial fusion in mammalian cells. J Cell Sci 116: 2763–2774.
19. Chen H, Detmer SA, Ewald AJ, Griffin EE, Fraser SE, et al. (2003) Mitofusins Mfn1 and Mfn2 coordinately regulate mitochondrial fusion and are essential for embryonic development. J Cell Biol 160: 189–200.
20. Cipolat S, Martins de Brito O, Dal Zilio B, Scorrano L (2004) OPA1 requires mitofusin 1 to promote mitochondrial fusion. Proc Natl Acad Sci U S A 101: 15927–15932.
21. Ishihara N, Nomura M, Jofuku A, Kato H, Suzuki SO, et al. (2009) Mitochondrial fission factor Drp1 is essential for embryonic development and synapse formation in mice. Nat Cell Biol 11: 958–966.
22. Yoneyama M, Kikuchi M, Matsumoto K, Imaizumi T, Miyagishi M, et al. (2005) Shared and unique functions of the DExD/H-box helicases RIG-I, MDA5, and LGP2 in antiviral innate immunity. J Immunol 175: 2851–2858.

23. Moore CB, Bergstralh DT, Duncan JA, Lei Y, Morrison TE, et al. (2008) NLRX1 is a regulator of mitochondrial antiviral immunity. Nature 451: 573–577.
24. Tang ED, Wang CY (2009) MAVS self-association mediates antiviral innate immune signaling. J Virol 83: 3420–3428.
25. Yasukawa K, Oshiumi H, Takeda M, Ishihara N, Yanagi Y, et al. (2009) Mitofusin 2 inhibits mitochondrial antiviral signaling. Sci Signal 2: ra47.
26. Castanier C, Garcin D, Vazquez A, Arnoult D (2010) Mitochondrial dynamics regulate the RIG-I-like receptor antiviral pathway. EMBO Rep 11: 133–138.
27. Fujita T (2009) A nonself RNA pattern: tri-p to panhandle. Immunity 31: 4–5.
28. Alberts B, Johnson A, Lewis J, Raff M, Roberts K (2008) Energy Conversion: Mitochondria and Chloroplasts. Molecular Biology of the Cell, Fifth Edition. New York: Garland Science. pp 813–878.
29. Yoneyama M, Suhara W, Fukuhara Y, Sato M, Ozato K, et al. (1996) Autocrine amplification of type I interferon gene expression mediated by interferon stimulated gene factor 3 (ISGF3). J Biochem 120: 160–169.
30. Kaukinen P, Sillanpaa M, Kotenko S, Lin R, Hiscott J, et al. (2006) Hepatitis C virus NS2 and NS3/4A proteins are potent inhibitors of host cell cytokine/chemokine gene expression. Virol J 3: 66.

Hepatology Research

Hepatology Research 2010; **40**: 1248–1253 doi: 10.1111/j.1872-034X.2010.00730.x

Short Communication

Gene expression profile of Li23, a new human hepatoma cell line that enables robust hepatitis C virus replication: Comparison with HuH-7 and other hepatic cell lines

Kyoko Mori,* Masanori Ikeda, Yasuo Ariumi and Nobuyuki Kato*

Department of Tumor Virology, Okayama University Graduate School of Medicine, Dentistry and Pharmaceutical Sciences, Okayama, Japan

Aim: Human hepatoma cell line HuH-7-derived cells are currently the only cell culture system used for robust hepatitis C virus (HCV) replication. We recently found a new human hepatoma cell line, Li23, that enables robust HCV replication. Although both cell lines had similar liver-specific expression profiles, the overall profile of Li23 seemed to differ considerably from that of HuH-7. To understand this difference, the expression profile of Li23 cells was further characterized by a comparison with that of HuH-7 cells.

Methods: cDNA microarray analysis using Li23 and HuH-7 cells was performed. Li23-derived ORL8c cells and HuH-7-derived RSc cells, in which HCV could infect and efficiently replicate, were also used for the microarray analysis. For the comparative analysis by reverse transcription polymerase chain reaction (RT–PCR), human hepatoma cell lines (HuH-6, HepG2, HLE, HLF and PLC/PRF/5) and immortalized hepatocyte cell line (PH5CH8) were also used.

Results: Microarray analysis of Li23 versus HuH-7 cells selected 80 probes to represent highly expressed genes that have ratios of more than 30 (Li23/HuH-7) or 20 (HuH-7/Li23). Among them, 17 known genes were picked up for further analysis. The expression levels of most of these genes in Li23 and HuH-7 cells were retained in ORL8c and RSc cells, respectively. Comparative analysis by RT–PCR using several other hepatic cell lines resulted in the classification of 17 genes into three types, and identified three genes showing Li23-specific expression profiles.

Conclusion: Li23 is a new hepatoma cell line whose expression profile is distinct from those of frequently used hepatic cell lines.

Key words: hepatitis C virus, hepatoma cell line, HuH-7, Li23, microarray

INTRODUCTION

HUH-7, A HUMAN hepatoma cell line,[1] is frequently used in the research of hepatitis C virus (HCV), since an HCV replicon system enabling HCV subgenomic RNA replication was developed using HuH-7 cells.[2] Even with the use of an efficient HCV production system developed in 2005,[3] HuH-7-derived cells are still used as the only cell line for persistent HCV production systems.

Correspondence: Professor Nobuyuki Kato, Department of Tumor Virology, Okayama University Graduate School of Medicine, Dentistry and Pharmaceutical Sciences, Okayama 700-8558, Japan. Email: nkato@md.okayama-u.ac.jp

*These authors contributed equally to this work.

Received 21 July 2010; revision 16 August 2010; accepted 17 August 2010.

We previously developed HCV replicon systems[4,5] and an HCV production system[6] using HuH-7-derived cells. Furthermore, we recently found a new human hepatoma cell line, Li23, that enables robust HCV RNA replication and persistent HCV production.[7] In that study, using microarray analysis, we excluded the possibility that the obtained Li23-derived cells were derived from contamination of HuH-7-derived cells used for HCV replication.[7] In addition, we noticed that the gene expression profile of Li23 cells seemed considerably different from that of HuH-7 cells. Therefore, we assumed that the Li23 cell line possesses a unique expression profile among widely used human hepatoma cell lines. To evaluate this assumption, we further characterized the expression profile of Li23 cells by comparing it with those of other human hepatoma cell lines, including HuH-7,[1] HuH-6,[8] HepG2,[9] HLE,[10] HLF[10] and PLC/PRF/5.[11] Human immortalized hepatocyte cell line

PH5CH8[12] was also used for the comparison. Here, we show that the Li23 cell line possesses a distinct expression profile among hepatic cell lines.

METHODS

Cell culture

HUH-7, HUH-6, HEPG2, HLE, HLF and PLC/PRF/5 cells were cultured in Dulbecco's modified Eagle's medium supplemented with 10% fetal bovine serum. Li23 and PH5CH8 cells were maintained as described previously.[7] Cured cells (Li23-derived ORL8c and HuH-7-derived RSc), from which the HCV RNA had been eliminated by interferon (IFN) treatment, were also maintained as described previously.[7]

cDNA microarray analysis

Li23, ORL8c, HuH-7 and RSc cells (1×10^6 each) were plated onto 10-cm diameter dishes and cultured for 2 days. Total RNA from these cells were prepared using the RNeasy extraction kit (QIAGEN, Hilden, Germany). cDNA microarray analysis was performed according to the methods described previously.[7] Differentially expressed genes were selected by comparing the arrays from Li23 and HuH-7 cells. The selected genes were further compared with the array from ORL8c or RSc cells.

Reverse transcription polymerase chain reaction

Reverse transcription polymerase chain reaction (RT–PCR) was performed to detect cellular mRNA as described previously.[13] Briefly, total RNA (2 μg) was reverse-transcribed with M-MLV reverse transcriptase (Invitrogen, San Diego, CA, USA) using an oligo dT primer (Invitrogen) according to the manufacturer's protocol. One-tenth of the synthesized cDNA was used for PCR. The primers arranged for this study are listed in Table 1. In addition, we used primer sets for New York esophageal squamous cell carcinoma 1 (NY-ESO-1), β-defensin-1 (DEFB1), lectin, galactoside-binding, soluble 3 (LGALS3)/Galectin-3, melanoma-specific antigen family A6 (MAGEA6), UDP glycosyltransferase 2 family polypeptide B4 (UGT2B4), transmembrane 4 superfamily member 3 (TM4SF3), insulin-like growth factor binding protein 2 (IGFBP2), arylacetamide deacetylase (AADAC), albumin and glyceraldehyde-3-phosphate dehydrogenase (GAPDH), as described previously.[7]

RESULTS

Genes showing pronounced differences in gene expression between Li23- and HuH-7-derived cells

WE RECENTLY ESTABLISHED several Li23-derived cell lines showing robust HCV RNA replication.[7] In convenient microarray analysis using these cell lines, we noticed that the gene expression profile of Li23 cells differed considerably from that of HuH-7 cells, and that several genes, including cancer antigens such as NY-ESO-1 and MAGEA6, were highly expressed in Li23 cells but were not expressed in HuH-7 cells.[7] However, it

Table 1 Primers used for reverse transcription polymerase chain reaction analysis

Gene (accession no.)	Direction	Nucleotide sequence (5′–3′)	Products (bp)
Cancer antigen 45, A5	Forward	TGGAGATGACCTAGAATGCAG	218
(CT45A5); NM_001007551	Reverse	CTCGTCTCATACATCTTGCTG	
Four-and-a-half LIM domain 1	Forward	GGAATCACTTACCAGGATCAG	243
(FHL1; NM_001449)	Reverse	TTTGCAGTGGAAGCAGTAGTC	
Thymosin β4, X-linked	Forward	ACCAGACTTCGCTCGTACTC	179
(TMSB4X; NM_021109)	Reverse	TCGCCTGCTTGCTTCTCCTG	
Lectin, galactoside-binding, soluble 1	Forward	CAACACCATCGTGTGCAACAG	253
(LGALS1; NM_002305)	Reverse	CAGCTGCCATGTAGTTGATGG	
Interferon-induced transmembrane protein 2	Forward	CCTCTTCATGAACACCTGCTG	184
(IFITM2; NM_006435)	Reverse	CACTGGGATGATGATGAGCAG	
Apolipoproteins A1	Forward	ACTGTGTACGTGGATGTGCTC	273
(APOA1; X02162)	Reverse	CTTCTTCTGGAAGTCGTCCAG	
α-2-HS-glycoprotein	Forward	AACCGAACTGCGATGATCCAG	248
(AHSG; NM_001622)	Reverse	TTCGACAGCATGCTCCTTCAG	
Gap junction protein-α 1	Forward	CATCTTCATGCTGGTGGTGTC	253
(GJA1; NM_000165)	Reverse	GTTTCTGTCGCCAGTAACCAG	

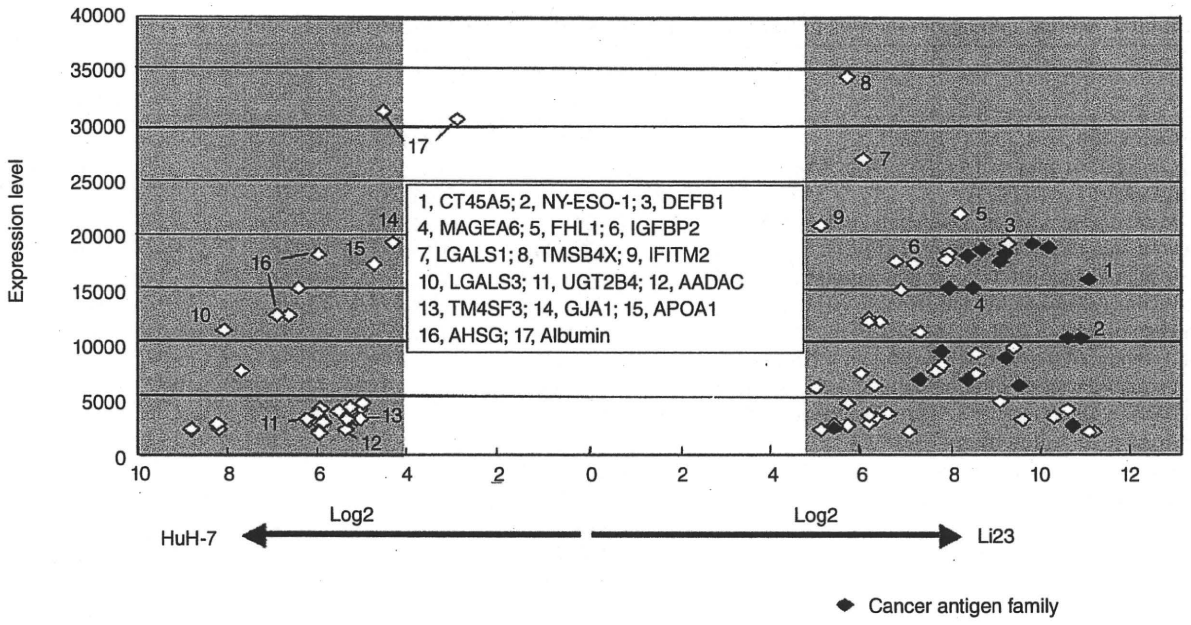

Figure 1 Genes showing pronounced differences in gene expression between Li23 and HuH-7 cells. The probes showing expression levels of more than 2000 and ratios of more than 30 (Li23/HuH-7) or 20 (HuH-7/Li23) are presented.

is unclear whether the expression profiles of these genes are characteristics of Li23 cells.

To clarify this point, comprehensive microarray analysis using Li23 and HuH-7 cells was performed. This revealed 4119 and 3570 probes whose expression levels were upregulated and downregulated at ratios of more than 2 and less than 0.5 in Li23 versus HuH-7 cells, respectively. From among these probes, we selected those showing ratios of more than 30 (Li23/HuH-7) and 20 (HuH-7/Li23), and further selected the probes showing expression levels of more than 2000 (actual value of measurement). By these selections, 80 probes were assigned (Fig. 1). The most distinguishing characteristic of the comparison is that the cancer antigen family (18 probes) was highly expressed in Li23 cells but was not highly expressed in HuH-7 cells (Fig. 1). From these probes, 14 known genes showing expression levels above 10 000 (#1–10 and #14–17 in Fig. 1) and three additional known genes (#11–13 in Fig. 1) were chosen as representative genes for further analysis.

Regarding the total of 17 genes, the expression levels in Li23 versus ORL8c or HuH-7 versus RSc were compared. The expression levels of most of the 17 genes were maintained between Li23 and ORL8c cells or between HuH-7 and RSc cells (Table 2). These results indicate that ORL8c and RSc cells retained the characteristics of parent Li23 and HuH-7 cells, respectively. However, it was notable that the expression levels of apolipoprotein A1 (APOA1), α-2-HS-glycoprotein (AHSG), and albumin were significantly higher in ORL8c cells than in Li23 cells, suggesting that ORL8c is selected as a specific clone from Li23 cell populations.

Expression profiles of representative genes whose expression levels showed drastic differences between Li23 and HuH-7 cells among human hepatic cell lines

Regarding the 17 genes selected above, we performed comparative analyses by RT–PCR using Li23, HuH-7, HuH-6, HepG2, HLE, HLF, PLC/PRF/5 and PH5CH8 cells in order to clarify whether or not these genes exhibit Li23-specific expression profiles. The results of the RT–PCR performed after optimization of PCR conditions in each gene resulted in the classification of the 17 genes into three types (A, B and C in Fig. 2). NY-ESO-1 and DEFB1 (high expression in Li23 only), and LGALS3/Galectin-3 (no expression in Li23 only) belonged to type A, which showed a Li23-specific feature. Type B showed that the expression levels in Li23, HLE, HLF, PLC/PRF/5 and/or PH5CH8 cells were greatly higher or lower than those in HuH-7, HuH-6 and HepG2 cells. Type B consisted of cancer antigen 45, A5

Table 2 Representative genes showing pronounced differences in gene expression between Li23 and HuH-7 cells

Gene	Accession no.	Li23	Li23-derived ORL8c	HuH-7	HuH-7-derived RSc
Cancer antigen 45, A5 (CT45A5)	NM_001007551	15 857†	10 508	8	23
Cancer testis antigen 1A (NY-ESO-1/CTAG1A)	U87459	9 005	5 503	5	8
β-Defensin-1 (DEFB1)	U73945	18 311	8 326	31	7
Melanoma-specific antigen family A6 (MAGEA6)	U10691	15 168	17 050	42	35
Four-and-a-half LIM domain 1 (FHL1)	NM_001449	21 851	13 428	77	79
Insulin-like growth factor binding protein 2 (IGFBP2)	NM_000597	17 429	8 931	117	13
Lectin, galactoside-binding, soluble 1 (LGALS1)	NM_002305	26 694	27 098	379	11
Thymosin β4, X-linked (TMSB4X)	NM_021109	34 273	26 199	648	307
IFN-induced transmembrane protein 2 (IFITM2)	NM_006435	20 762	9 645	595	637
Lectin, galactoside-binding, soluble 3 (LGALS3/Galectin 3)	BC001120	41	70	10 973	6 020
UDP glycosyltransferase 2 family polypeptide B4 (UGT2B4)	NM_021139	40	57	2 863	7 546
Arylacetamide deacetylase (AADAC)	NM_001086	57	73	2 282	4 746
Transmembrane 4 superfamily member 3 (TM4SF3)	NM_004616	95	51	3 220	1 265
Gap junction protein-α 43 KDa (GJA1)	NM_000165	951	2	19 090	19 485
Apolipoprotein A1 (APOA1)	X02162	673	7 230	16 920	15 202
α-2-HS-glycoprotein (AHSG)	NM_001622	308	6 373	18 436	26 000
Albumin	AF116645	4 304	30 111	30 234	33 140
	D16931	1 387	23 615	30 668	39 144

†Signal intensity in human genome U133 Plus 2.0 array.

(CT45A5), MAGEA6, four-and-a-half LIM domains 1 (FHL1), Thymosin B4, X-linked (TMSB4X), lectin, galactoside-binding, soluble 1 (LGALS1) and IFN-induced transmembrane protein 2 (IFITM2) – all of which were highly expressed in Li23 cells – and APOA1, AHSG and UGT2B4, which were highly expressed in HuH-7 cells. The remaining five genes were assigned to type C and showed more complex expression profiles (Fig. 2). For instance, Gap junction protein-α 43 kDa (GJA1) expression was observed in HuH-7, HLE, HLF, PLC/PRF/5 and PH5CH8 cell lines, but not in Li23, HuH-6 or HepG2 cell lines. In addition, IGFBP2 expression was observed in Li23, HuH-6 and PH5CH8 cell lines, but not in the other cell lines. Together, these results indicate that the Li23 cell line possesses a distinct expression profile among frequently used hepatic cell lines.

DISCUSSION

IN THIS STUDY, we assigned 17 known genes that showed drastic differences between Li23 and HuH-7 cells, and classified the expression profiles of these genes into at least three types among frequently used hepatic cell lines. Three genes (NY-ESO-1, DEFB1 and LGALS3/Galectin-3) were identified as the representative showing Li23-specific expression.

NY-ESO-1 is a well-characterized cancer-testis antigen (CTAG) that appears to be the most immunogenic CTAG known to date.[14] NY-ESO-1 is expressed in malignant tumors such as melanoma, lung carcinoma and bladder cancer, which are called "CTAG-rich" tumor types, but are expressed solely in the testis among normal adult tissues.[15] Because a spontaneous immune response to NY-ESO-1 is frequently observed in patients with malignant tumors including hepatocellular carcinoma,[16] cancer vaccine trials based on NY-ESO-1 are currently underway.[15] However, the biological role of NY-ESO-1 in both tumors and testis remains poorly understood. Accordingly, the Li23 cell line may be useful for the study of the biological role of NY-ESO-1.

Human defensins, which are small cationic peptides produced by neutrophils and epithelial cells, form two genetically distinct subfamilies, α-defensin and β-defensin. DEFB1, identified in this study, is one of six members belonging to β-defensins and appears to be involved in the antimicrobial defense of the epithelia of surfaces.[16,17] Although α-defensins consisting of six members are known to be expressed in a variety of tumors, DEFB1 is downregulated in some tumor types in which it could behave as a tumor suppressor protein.[18] Our study revealed that except DEFB1 in Li23 cells, no α- or β-defensin members were expressed in the

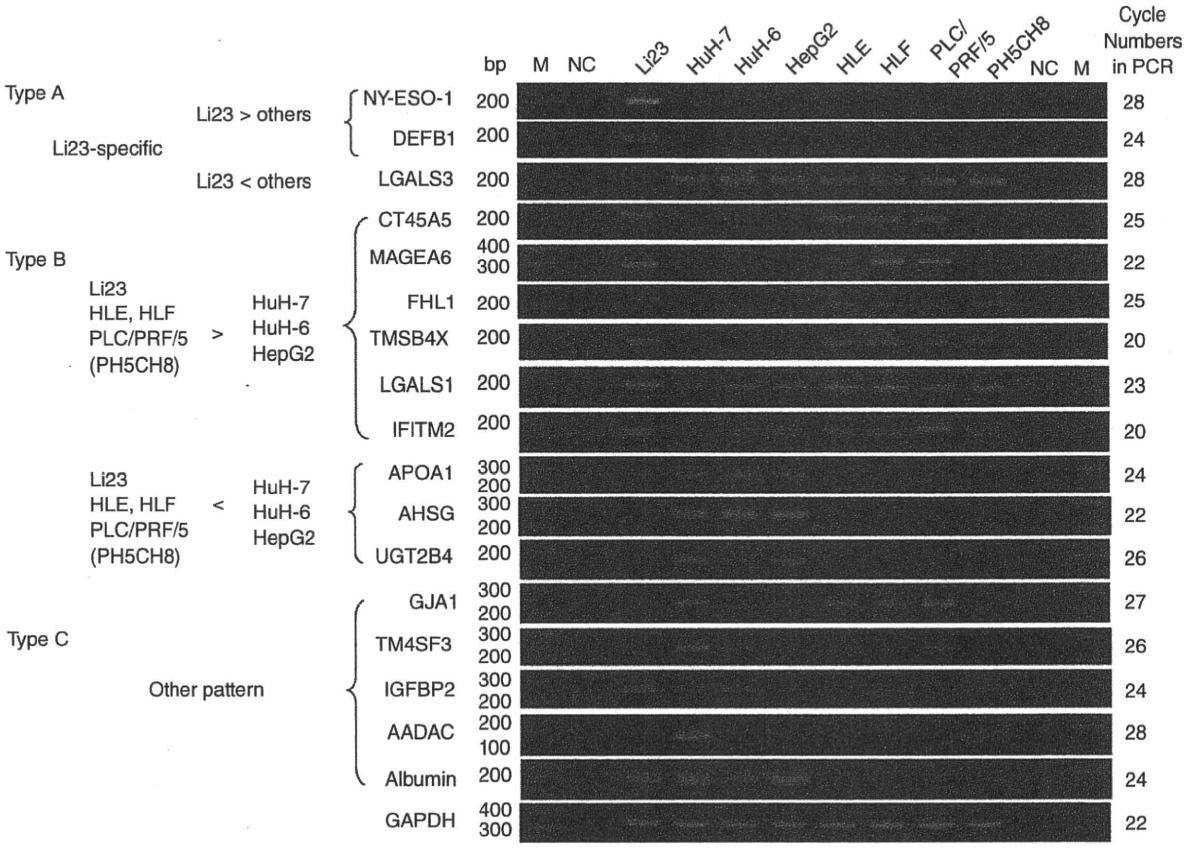

Figure 2 Expression profiles of representative genes, whose expression levels showed drastic differences between Li23 and HuH-7 cells, among human hepatic cell lines. Reverse transcription polymerase chain reaction (RT–PCR) analysis was performed as described in Methods. PCR products were detected by staining with ethidium bromide after separation by electrophoresis on 3% agarose gels.

hepatic cell lines tested in this study (data not shown). Because the molecular mechanism underlying DEFB1 expression or its role in oncogenesis remains to be clarified, Li23 cells may be useful for a study like that.

LGALS3/Galectin-3 is the most studied member of the galectin family, which is characterized by specific binding of β-galactosides through the carbohydrate-recognition domain.[19] LGALS3/Galectin-3 is ubiquitously expressed in numerous cell and tissue types; it is located in both nuclei and cytoplasm, and is secreted through a non-classical pathway. To date, LGALS3/Galectin-3 was found to be involved in many regulations including development, immune reaction, tumorigenesis, and tumor growth and metastasis.[19,20] Indeed, the overexpression of LGALS3/Galectin-3 in cirrhotic and hepatocellular carcinoma has also been reported.[21] In such situations, the absence of LGALS3/Galectin-3 expression in the Li23 cell line is a unique feature among hepatic cell lines, which show high expression levels. Accordingly, the Li23 cell line might be useful as a LGALS3/Galectin-3-null cell line for various studies including those on tumor growth and metastasis.

Although we identified Li23-specific genes showing distinct expression levels among hepatic cell lines examined, microarray analysis revealed that the expression profiles of Li23 and HuH-7 cells, both of which possess an environment for robust HCV replication, differed considerably. Accordingly, such differences may affect the properties or multiplications of HCV, such as susceptibility to anti-HCV reagents, the mutation rate of the HCV genome and the efficiency of HCV replication. Further comparative analysis using Li23 and HuH-7 cells will help to resolve these uncertain subjects.

ACKNOWLEDGMENTS

WE THANK NAOKO Kawahara for her technical assistance. This work was supported by a Grant-in-Aid for research on hepatitis from the Ministry of Health, Labor and Welfare of Japan. K. M. was supported by a Research Fellowship from the Japan Society for Promotion of Science for Young Scientists.

REFERENCES

1 Nakabayashi H, Taketa K, Miyano K, Yamane T, Sato J. Growth of human hepatoma cells lines with differentiated functions in chemically defined medium. *Cancer Res* 1982; **42**: 3858–63.
2 Lohmann V, Körner F, Koch J-O, Herian U, Theilman L, Bartenschlager R. Replication of subgenomic hepatitis C virus RNAs in a hepatoma cell line. *Science* 1999; **285**: 110–13.
3 Wakita T, Pietschmann T, Kato T *et al.* Production of infectious hepatitis C virus in tissue culture from a cloned viral genome. *Nat Med* 2005; **11**: 791–6.
4 Kato N, Sugiyama K, Namba K *et al.* Establishment of a hepatitis C virus subgenomic replicon derived from human hepatocytes infected in vitro. *Biochem Biophys Res Commun* 2003; **306**: 756–66.
5 Ikeda M, Abe K, Dansako H, Nakamura T, Naka K, Kato N. Efficient replication of a full-length hepatitis C virus genome, strain O, in cell culture, and development of a luciferase reporter system. *Biochem Biophys Res Commun* 2005; **329**: 1350–9.
6 Ariumi Y, Kuroki M, Abe K *et al.* DDX3 DEAD-box RNA helicase is required for hepatitis C virus RNA replication. *J Virol* 2007; **81**: 13922–6.
7 Kato N, Mori K, Abe K *et al.* Efficient replication systems for hepatitis C virus using a new human hepatoma cell line. *Virus Res* 2009; **146**: 41–50.
8 Tokiwa T, Doi I, Sato J. Preparation of single cell suspensions from hepatoma cells in culture. *Acta Med Okayama* 1975; **29**: 147–50.
9 Aden DP, Fogel A, Plotkin S, Damjanov I, Knowles BB. Controlled synthesis of HBsAg in a differentiated human liver carcinoma-derived cell line. *Nature* 1979; **282**: 615–16.
10 Doi I, Nambe M, Sato J. Establishment and some biological characteristics of human hepatoma cell lines. *Gann* 1975; **66**: 385–92.
11 Alexander JJ, Bey EM, Geddes EW, Lecatsaa G. Establishment of a continuously growing cell line from primary carcinoma of the liver. *S Afr Med J* 1976; **50**: 2124–8.
12 Ikeda M, Sugiyama K, Mizutani T *et al.* Human hepatocyte clonal cell lines that support persistent replication of hepatitis C virus. *Virus Res* 1998; **56**: 157–67.
13 Dansako H, Naganuma A, Nakamura T, Ikeda F, Nozaki A, Kato N. Differential activation of interferon-inducible genes by hepatitis C virus core protein mediated by the interferon stimulated response element. *Virus Res* 2003; **97**: 17–30.
14 Yoshida N, Abe H, Ohkuri T *et al.* Expression of the MAGE-A4 and NY-ESO-1 cancer-testis antigens and T cell infiltration in non-small cell lung carcinoma and their prognostic significance. *Int J Oncol* 2006; **28**: 1089–98.
15 Caballero OL, Chen YT. Cancer/testis (CT) antigens: potential targets for immunotherapy. *Cancer Sci* 2009; **100**: 2014–21.
16 Korangy F, Ormandy LA, Bleck JS *et al.* Spontaneous tumor-specific humoral and cellular immune responses to NY-ESO-1 in hepatocellular carcinoma. *Clin Cancer Res* 2004; **10**: 4332–41.
17 Bensch KW, Raida M, Magert HJ, Schulz-Knappe P, Forssmann WG. HBD-1: a novel bta-defensin from human plasma. *FEBS Lett* 1995; **368**: 331–5.
18 Droin N, Hendra JB, Ducoroy P, Solary E. Human defensins as cancer biomarkers and antitumour molecules. *J Proteomics* 2009; **72**: 918–27.
19 Dumic J, Dabelic S, Flögel M. Galectin-3: an open-ended story. *Biochim Biophys Acta* 2006; **1760**: 616–35.
20 Danguy A, Camby I, Kiss R. Galectins and cancer. *Biochim Biophys Acta* 2002; **1572**: 285–93.
21 Hsu DK, Dowling CA, Jeng KC, Chen JT, Yang RY, Liu FT. Galectin-3 expression is induced in cirrhotic liver and hepatocellular carcinoma. *Int J Cancer* 1999; **81**: 519–26.

Journal of Bioscience and Bioengineering
VOL. 110 No. 3, 374–376, 2010

ELSEVIER

www.elsevier.com/locate/jbiosc

TECHNICAL NOTE

Generation of single-chain Fvs against detergent-solubilized recombinant antigens with a simple coating procedure

Torahiko Tanaka,[1,*] Yuichiro Hasegawa,[2,3] Makoto Saito,[2,3] Masanori Ikeda,[4] and Nobuyuki Kato[4]

Department of Advanced Medical Science, Nihon University School of Medicine, 30-1 Oyaguchi-kamimachi, Itabashi, Tokyo 173-8610, Japan[1]
Department of Obstetrics and Gynecology, Nihon University School of Medicine, 30-1 Oyaguchi-kamimachi, Itabashi, Tokyo 173-8610, Japan[2]
Open Research Center for Genome and Infectious Disease Control, Nihon University School of Medicine, 30-1 Oyaguchi-kamimachi, Itabashi, Tokyo 173-8610, Japan[3] *and Department of Tumor Virology, Okayama University Graduate School of Medicine, Dentistry, and Pharmaceutical Sciences, 2-5-1 Shikata-cho, Okayama 700-8558, Japan*[4]

Received 5 February 2010; accepted 29 March 2010

Antigen coating on polystyrene is prevented by detergent. We present here a simple procedure to coat detergent-solubilized antigen for subsequent panning selection of single-chain Fv (scFv), the target antigen of which was the hepatitis C virus (HCV) non-structural protein (NS) 4B, an integral membrane protein.

[**Key words:** Single-chain Fv; Detergent; Critical micelle concentration; Hepatitis C virus; NS4B]

The single-chain Fv (scFv)-phage display (1) is a useful technology to obtain antibodies against a wide category of antigens, including non-protein antigens, autoantigens, and antigens that are difficult to generate in animals. To obtain specific scFvs, panning selection has been performed on antigen-coated polystyrene using an scFv-phage display library (2). Antigen coating is achieved by the simple incubation of a soluble antigen solution in polystyrene tubes and wells. However, when an antigen is detergent-solubilized, detergent severely disturbs antigen coating on polystyrene (3,4) and this becomes an obstacle to the panning selection of scFv. To overcome the problem, we developed a simple procedure to coat an antigen by lowering the detergent concentration in an antigen solution with no additional material or time-consuming work. The target antigen was the hepatitis C virus (HCV) non-structural protein (NS) 4B, an integral membrane protein. HCV has a positive-stranded RNA genome encoding at least 10 viral proteins, namely, a core, E1, E2, p7, NS2, NS3, NS4A, NS4B, NS5A, and NS5B (5). The 5' untranslated region has a functional internal ribosome entry site, and the 3' untranslated region contains a highly conserved 98 nucleotide structure, the 3' X (6), which is indispensable for the viral genome replication. The NS proteins are thought to form complexes to replicate the viral genome. Little is known about the role of NS4B which harbors at least four transmembrane domains. Anti-NS4B scFvs to various epitopes are a useful tool for analyzing the roles of NS4B in virus replication.

We prepared the N-terminal hexahistidine (His)-tagged NS4B (NS4BHis) as an antigen based on the sequence of strain O (subtype 1b HCV) (7) using the pET expression system (Novagen, USA). The NS4B fragment was amplified by PCR using the restriction-site-tagged primers 5'-TTACATATGCATCACCACCATCACCATGGTGCCTCGCACC-TCCCTTAC-3' (with the *Nde*I site as underlined) and 5'-TTAGGATCCT-TAGCATGGCGTGGAGCAGTC-3' (with the *Bam*HI site as underlined) with a plasmid pON/C-5B/KE (7) as a template. The expression construct was created by ligating the *Nde*I–*Bam*HI-digested fragment of NS4B into the *Nde*I–*Bam*HI-digested pET3a vector. Similarly, the N-terminal Myc (EQKLISEEDL)-His-tagged NS4B (NS4BMycHis) construct was created by PCR using the primers 5'-TTACATATGGAACA-GAAACTGATTAGCGAAGAAGATCTGCATCACCACCATCACCATG-3' (with the *Nde*I site as underlined) and 5'-TTAGGATCCTTAGCATGGCGTGGAG-CAGTC-3' (with the *Bam*HI site as underlined) with the NS4BHis construct as the PCR template. NS4B proteins were expressed in *Escherichia coli* strain KRX (Promega, USA) in the presence of 0.1% rhamnose at 25 °C. The cells were suspended in a buffer containing 10 mM Tris–HCl, pH 7.4, 5 mM EDTA, and a Complete™ protease inhibitor cocktail (Roche, Germany), sonicated three times with 5 s bursts, and centrifuged at 5000g for 3 min. Because NS4BHis was recovered in the pellet, the solubilization conditions were examined. NS4BHis was efficiently solubilized in the presence of 0.5 M NaCl with 1% n-dodecyl β-D-maltoside (DDM) or Triton X-100 but not with Tween-20 and n-octyl β-D-glucoside (OG). After solubilization with DDM, NS4BHis was affinity-purified using Ni NTA agarose (Qiagen, USA) to near-homogeneity according to the manufacturer's protocol.

In the usual panning selection of antigen-specific scFv, the antigen is coated on polystyrene by simple incubation in an aqueous buffer. In the present work, the purified NS4BHis preparation contains 1% DDM, and, as described above, detergents are known to severely disturb antigen coating on polystyrene. Upon a preliminary experiment, we failed to efficiently coat NS4BHis with 50-fold simple dilution (final

* Corresponding author. Present address: Division of Biochemistry, Department of Biomedical Sciences, Nihon University School of Medicine, 30-1 Oyaguchi-kamimachi, Itabashi, Tokyo 173-8610, Japan. Tel.: +81 3 3972 8111x2241; fax: +81 3 3972 8199.
E-mail address: tanakat@med.nihon-u.ac.jp (T. Tanaka).

1389-1723/$ - see front matter © 2010, The Society for Biotechnology, Japan. All rights reserved.
doi:10.1016/j.jbiosc.2010.03.014

DDM, 0.02%) on polystyrene. We then modified the purification step to lower the DDM concentration. After NS4BHis was bound to Ni affinity resin, washing and elution were conducted using a buffer with a low but slightly higher than critical micelle concentration (CMC) of DDM (0.01%; the CMC of DDM is 0.0087%). In detail, the Ni affinity resin was pre-equilibrated with a TBS buffer (10 mM Tris–HCl, pH 7.4, 0.15 M NaCl) containing 0.01% DDM and 20 mM imidazole, and the solubilized NS4BHis sample (to which 20 mM imidazole was also added) was applied to the resin. The bound NS4BHis was washed first with a 10-bed volume of the same buffer for equilibration and then with a 10-bed volume of TBS-0.01% DDM-0.5 M NaCl-20 mM imidazole, pH 7.4. Finally, the bound NS4B was eluted with a three-bed volume of TBS-0.01% DDM-0.5 M NaCl-0.25 M imidazole, pH 7.4. Under these conditions, NS4BHis could be purified and concentrated efficiently. Interestingly, even with 0.005% DDM, NS4BHis was efficiently purified in a similar manner. By further 50-fold dilution with a detergent-free buffer (final DDM concentration, 0.0002%), the NS4BHis was found to be coated on polystyrene efficiently. Thus a simple coating protocol for detergent-solubilized antigens was established by a modification of purification procedure to lower detergent concentrations.

We examined the concentration limits of frequently used detergents, including DDM, which enable the coating of NS4BHis (Fig. 1). For this purpose, NS4BMycHis was prepared using the same purification protocol as for NS4BHis with 0.01% of DDM. The NS4BMycHis solution was incubated in polystyrene wells in a microtiter plate with or without various concentrations of detergent (NP40, Triton X-100, Tween-20, OG, and DDM). In this experiment, a 1 µl (2.5 µg) purified NS4BMycHis preparation containing 0.01% DDM was diluted to 50 µl with a TBS buffer for each well; thus, the coating solution contained 0.0002% of carry-over DDM. After 6 h of incubation, each well was blocked, and the amount of adsorbed NS4BMycHis was evaluated using an anti-myc antibody HRP conjugate and the peroxidase-dependent colorimetric

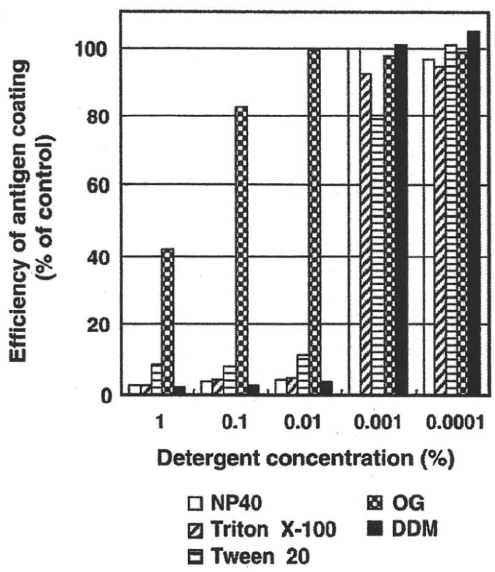

FIG. 1. The influence of various detergents on the coating of NS4B to microplate wells. All the reactions were carried out with final volume of 50 µl in microplate wells (Iwaki, Japan). NS4BMycHis (2.5 µg) was incubated for 6 h at room temperature in the absence or presence of an indicated concentration of detergent (NP 40, Triton X-100, Tween 20, OG, or DDM). The wells were washed 10 times with ultrapure water and blocked with a 5% skim milk-TBS buffer (MTBS) for 1 h. After washing, the wells were reacted with 200-fold diluted anti-myc antibody HRP conjugate (Wako Chemical, Japan) in 5% MTBS for 1 h. After washing, the wells were reacted with 2, 2'-azino-bis(3-ethylbenzthiazoline-6-sulfonic acid) (ABTS; Sigma, USA) according to manufacturer's protocol and the absorbance at 405 nm was determined. Data are the mean of two independent experiments and shown as a % of the control value obtained in the absence of detergent.

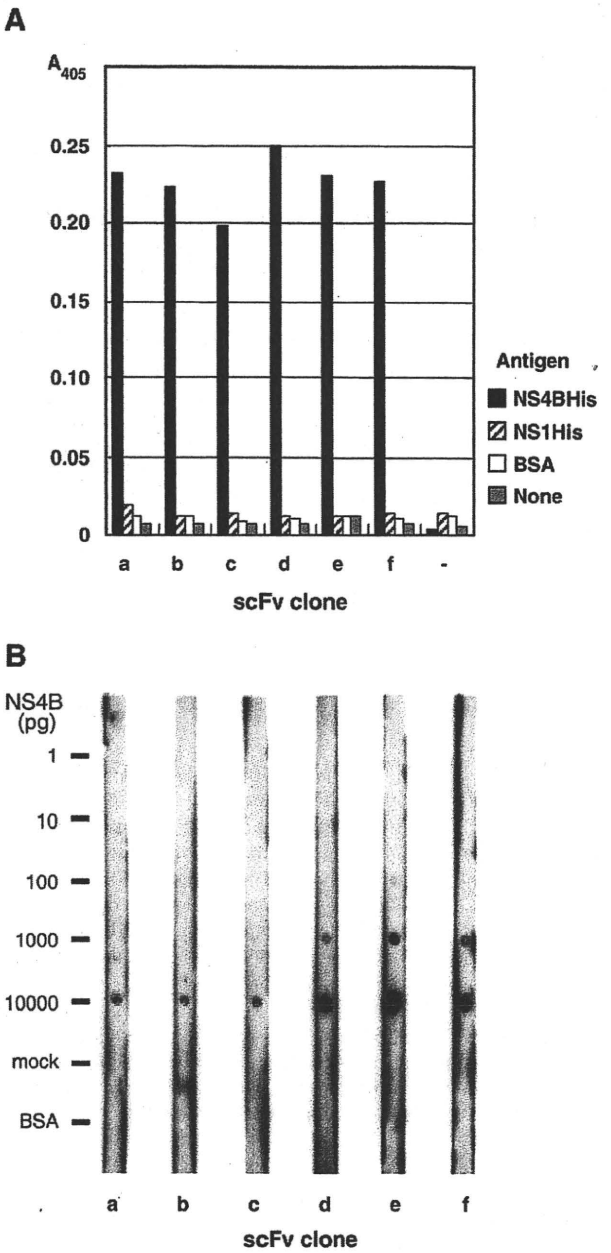

FIG. 2. Specificity and sensitivity assays of scFv phage clones against NS4B. (A) Confirmation of the antigen specificity by ELISA. All the reactions were carried out with final volume of 50 µl in each well. Indicated antigens (1 µg in TBS buffer); NS4BHis (containing 0.0002% DDM as final concentration), influenza virus NS1His (8), and bovine serum albumin (BSA) or TBS buffer alone (None), were incubated in wells of a microplate at 4 °C overnight. The wells were washed 10 times with ultrapure water and blocked with a 5% MTBS for 1 h. The wells were then incubated with or without (−) phage clones (a to f, 2.5×10^9 cfu in 5% MTBS) for 1 h, followed by incubation with 10,000-fold dilution of anti-M13 antibody HRP conjugate (GE, USA) in 5% MTBS for 30 min. Reaction was developed with ABTS and the absorbance at 405 nm was determined. (B) A sensitivity assay of scFv clones against NS4B. Indicated amounts of NS4BHis (0 [mock], 1, 10, 100, 1000, and 10,000 pg) and BSA (10 ng) in 0.5 µl TBS-0.01% DDM were spotted on nitrocellulose strips, air-dried, and incubated in TBS-0.1% Tween-20 overnight. After washing with ultrapure water, the spots were blocked, reacted with scFv phage (5×10^{10} cfu/ml in 5% MTBS) for 1 h, and visualized using an anti-M13 antibody HRP (horseradish peroxidase) conjugate and the ECL-Plus Western Blotting Detection Kit (GE Healthcare, UK) as described previously (9,11).

method. As shown in Fig. 1, the addition of 0.01% or more detergent, except for OG, severely disturbed the coating of NS4BMycHis, while that of 0.001% or lower detergent did not; only when 0.001% Tween-20 was used was the coating slightly disturbed. The results suggest that antigens cannot be coated on polystyrene in the presence of these detergents under concentrations usually used for solubilization (0.1–1.0%). On the other hand, about 80% of coating efficiency was achieved under 0.1% OG, suggesting that OG is convenient for solubilization of antigens to be coated on polystyrene as far as it efficiently solubilizes the target antigens (as described above, NS4B could not, unfortunately, be solubilized efficiently with OG). An antigen solution containing 1% OG would be coated efficiently by simple dilution.

Then we carried out the selection of scFvs against NS4B from a human naive scFv phage display library (2.6×10^9 clones) (8) by usual panning protocol (2) with minor modifications. Polystyrene tubes (Maxisorp™, Nunc) were coated with NS4BHis (10 μg/ml in TBS buffer containing 0.0001% DDM as final concentration) and used for the selection. After blocking with 5% skim milk-TBS buffer (MTBS) for 1 h, the library phage (1×10^{12} cfu/ml of 5% MTBS) were incubated with the antigen for 1 h. After washing with TBS-0.1% Tween-20 for 10 times and then with TBS for 3 times, phage were eluted with 1.4% triethylamine and neutralized with a half volume of 1 M Tris–HCl pH 7.4. The phage were amplified in TG1 and used for the subsequent panning selection in the same manner. The reaction volume for antigen coating and phage reaction was 2 ml for the first round and 1 ml for the second and third round selections. After three rounds of selection, 6 independent clones (a to f) were obtained based on *Hae*III fingerprinting of the Fv region (9). Sequencing of the Fv region confirmed that these 6 clones were distinct (data not shown). The antigen specificity of the clones was confirmed by enzyme-linked immunosorbent assay (ELISA). As shown in Fig. 2A, all of the 6 clones reacted with NS4BHis but not with unrelated proteins such as bovine serum albumin (BSA) and unrelated His-tagged protein, influenza virus NS1His (8). The clones also did not react with uncoated wells. Thus the selected clones are specific to NS4B. To conveniently evaluate the sensitivity of selected scFvs, we spotted NS4BHis (1, 10, 100, 1000, 10,000 pg) and BSA (10 ng, as a negative control) on a nitrocellulose membrane and used it for dot blot analysis (Fig. 2B). Clones d, e, and f detected until the 1000 pg spot, and clones a, b, and c detected until the 10,000 pg spot. No clones detected the BSA spot. In our experience, scFv phages which can detect 100–10,000 pg of antigen spots were usually obtained by panning selection using a polystyrene-coated soluble antigen which was prepared without detergent. This suggests that the clones obtained in this work using a detergent-solubilized antigen were in a similar range of antigen affinity to clones against other soluble antigens obtained without detergent.

As described, the problem in the panning selection of scFv against detergent-solubilized antigens is more severe with low-CMC detergents, such as Triton X-100, as demonstrated by Gardas et al. (4), who found a strong correlation between the detergent CMC and the detergent concentration which inhibits protein binding to polystyrene. Presumably, the detergent micelle and protein molecule compete upon binding to polystyrene. This had also been suggested by Kenny et al. (10) when they showed that a higher molar ratio of antigen to detergent achieved a more efficient coating. The molecular structure and nature of detergents and proteins, such as hydrophobicity and hydrophilicity, may also affect which detergents and proteins have stronger affinities to polystyrene. In the present work, we found that the practical value of detergent concentration to enable efficient coating of a detergent-solubilized antigen is around 0.001% for frequently used low-CMC detergents, such as Triton X-100, Tween-20, NP40, and DDM. This value may also depend on the antigen concentration; we employed a relatively high antigen concentration (2.5 μg/50 μl = 50 μg/ml). Our procedure, in which the detergent concentration is lowered to a value near the CMC value during column work, is rapid and convenient to obtain a higher molar ratio of antigen to detergent. In this sense, our procedure is advantageous, especially when proteins are purified with affinity chromatography, since proteins are easily concentrated without an increase of the detergent concentration. Interestingly, even with the DDM concentration slightly lower than the CMC, recombinant NS4B was efficiently purified with Ni affinity chromatography. How low the detergent concentrations can be for target proteins to be efficiently purified may depend on the protein nature. Practically, researchers can easily evaluate whether a target protein can be purified well in detergent concentrations near CMC. In conclusion, if a target antigen can be solubilized by low-CMC detergent but not by high-CMC detergent, such as OG (CMC, 0.73%), as in the case of NS4B, our simple procedure is meaningful for the generation of scFv and other polystyrene-based work, such as the enzyme-linked immunosorbent assay and monoclonal antibody screening.

ACKNOWLEDGMENTS

This work was supported by a Nihon University Joint Research Grant, a grant from the Ministry of Education, Culture, Sports, Science, and Technology to promote open research for young academics and specialists, and the grant "Strategic Research Base Development" Program for Private Universities subsidized by MEXT (2008). We thank Dr. T. Hayashida (Northwestern University) for suggestions.

References

1. **Clackson, T., Hoogenboom, H. R., Griffiths, A. D., and Winter, G.:** Making antibody fragments using phage display libraries, Nature, **352**, 624–628 (1991).
2. **Griffiths, A. D., Williams, S. C., Hartley, O., Tomlinson, I. M., Waterhouse, P., Crosby, W. L., Kontermann, R. E., Jones, P. T., Low, N. M., and Allison, T. J., et al.:** Isolation of high affinity human antibodies directly from large synthetic repertoires, EMBO J., **13**, 3245–3260 (1994).
3. **Palfree, R. G. and Elliott, B. E.:** An enzyme-linked immunosorbent assay (ELISA) for detergent solubilized Ia glycoproteins using nitrocellulose membrane discs, J. Immunol. Methods, **52**, 395–408 (1982).
4. **Gardas, A. and Lewartowska, A.:** Coating of proteins to polystyrene ELISA plates in the presence of detergents, J. Immunol. Methods, **106**, 251–255 (1988).
5. **Kato, N.:** Molecular virology of hepatitis C virus, Acta Med. Okayama, **55**, 133–159 (2001).
6. **Tanaka, T., Kato, N., Cho, M. J., and Shimotohno, K.:** A novel sequence found at the 3' terminus of hepatitis C virus genome, Biochem. Biophys. Res. Commun., **215**, 744–749 (1995).
7. **Ikeda, M., Abe, K., Dansako, H., Nakamura, T., Naka, K., and Kato, N.:** Efficient replication of a full-length hepatitis C virus genome, strain O, in cell culture, and development of a luciferase reporter system, Biochem. Biophys. Res. Commun., **329**, 1350–1359 (2005).
8. **Murayama, R., Harada, Y., Shibata, T., Kuroda, K., Hayakawa, S., Shimizu, K., and Tanaka, T.:** Influenza A virus non-structural protein 1 (NS1) interacts with cellular multifunctional protein nucleolin during infection, Biochem. Biophys. Res. Commun., **362**, 880–885 (2007).
9. **Tanaka, T., Ito, T., Furuta, M., Eguchi, C., Toda, H., Wakabayashi-Takai, E., and Kaneko, K.:** In situ phage screening. A method for identification of subnanogram tissue components in situ, J. Biol. Chem., **277**, 30382–30387 (2002).
10. **Kenny, G. E. and Dunsmoor, C. L.:** Principles, problems, and strategies in the use of antigenic mixtures for the enzyme-linked immunosorbent assay, J. Clin. Microbiol., **17**, 655–665 (1983).
11. **Watanabe, N., Sasaoka, T., Noguchi, S., Nishino, I., and Tanaka, T.:** Cys669-Cys713 disulfide bridge formation is a key to dystroglycan cleavage and subunit association, Genes Cells, **12**, 75–88 (2007).

JOURNAL OF VIROLOGY, Sept. 2010, p. 9118–9127
0022-538X/10/$12.00 doi:10.1128/JVI.00402-10

Vol. 84, No. 18

A Disulfide-Bonded Dimer of the Core Protein of Hepatitis C Virus Is Important for Virus-Like Particle Production▽†

Yukihiro Kushima,[1,2] Takaji Wakita,[3] and Makoto Hijikata[1,2]*

Department of Viral Oncology, Institute for Virus Research, Kyoto University, Kyoto 606-8507, Japan[1]; Graduate School of Biostudies, Kyoto University, Kyoto 606-8507, Japan[2]; and Department of Virology II, National Institute of Infectious Diseases, Tokyo 162-8640, Japan[3]

Received 24 February 2010/Accepted 20 June 2010

Hepatitis C virus (HCV) core protein forms the nucleocapsid of the HCV particle. Although many functions of core protein have been reported, how the HCV particle is assembled is not well understood. Here we show that the nucleocapsid-like particle of HCV is composed of a disulfide-bonded core protein complex (dbc-complex). We also found that the disulfide-bonded dimer of the core protein (dbd-core) is formed at the endoplasmic reticulum (ER), where the core protein is initially produced and processed. Mutational analysis revealed that the cysteine residue at amino acid position 128 (Cys128) of the core protein, a highly conserved residue among almost all reported isolates, is responsible for dbd-core formation and virus-like particle production but has no effect on the replication of the HCV RNA genome or the several known functions of the core protein, including RNA binding ability and localization to the lipid droplet. The Cys128 mutant core protein showed a dominant negative effect in terms of HCV-like particle production. These results suggest that this disulfide bond is critical for the HCV virion. We also obtained the results that the dbc-complex in the nucleocapsid-like structure was sensitive to proteinase K but not trypsin digestion, suggesting that the capsid is built up of a tightly packed structure of the core protein, with its amino (N)-terminal arginine-rich region being concealed inside.

Hepatitis C virus (HCV) infection is a major cause of chronic hepatitis, liver cirrhosis, and hepatocellular carcinoma, affecting approximately 200 million people worldwide (13, 29, 44). Current treatment strategies, including interferon coupled with ribavirin, are not effective for all patients infected with HCV. An error-prone replication strategy allows HCV to undergo rapid mutational evolution in response to immune pressure and thus evade adaptive immune responses (10). New approaches to HCV therapy include the development of specifically targeted antiviral therapies for hepatitis C (STAT-Cs) which target such HCV proteins as the nonstructural 3/4A (NS3/4A), serine protease, and RNA-dependent RNA polymerase NS5B proteins (3). Despite the potent antiviral activities of some of these approaches, many resistant HCV strains have been reported after treatment with existing STAT-Cs (23, 48, 51). Therefore, identification of new targets that are common to all HCV strains and that are associated with low mutation rates is an area of active research.

HCV has a 9.6-kb, plus-strand RNA genome composed of a 5′ untranslated region (UTR), an open reading frame that encodes a single polyprotein of about 3,000 amino acids, and a 3′ UTR. The polyprotein is processed by host and viral proteases to produce three structural proteins (the core, envelope 1 [E1], and E2 proteins) and seven nonstructural proteins (the p7, NS2, NS3, NS4A, NS4B, NS5A, and NS5B proteins) (14, 16, 17, 22, 49). The HCV core protein is produced cotranslationally via carboxyl (C)-terminal cleavage to generate an immature core protein, 191 amino acids in length, on the endoplasmic reticulum (ER) (16). This protein consists of three predicted domains: the N-terminal hydrophilic domain (D1), the C-terminal hydrophobic domain (D2), and the tail domain (33), which serves as a signal peptide for the E1 protein. D1 includes a number of positively charged amino acids responsible for viral RNA binding (amino acids 1 to 75) (43) and the region involved in multimerization of the core protein via homotypic interactions (amino acids 36 to 91 and 82 to 102) (32, 40) (see Fig. S1 in the supplemental material). Hydrophobic D2 includes the region responsible for core protein association with lipid droplets (LDs; amino acids 125 to 144) (7, 18, 37), which accumulate in response to core protein production (1, 6).

Many functions of the core protein have been reported (13, 38, 50), yet because infectious HCV particles cannot be appropriately produced in currently available experimental systems, HCV particle assembly has not been elucidated to date. A cell culture system that reproduces the complete life cycle of HCV *in vitro* was developed by Wakita et al. using a cloned HCV genome (JFH1) (53). Using this system, the assembly of infectious HCV particles was found to occur near LDs and ER-derived LD-associated membranes (36, 47). Neither the structures nor the functions of the virus proteins involved in virus particle assembly are known, however. To elucidate this point, we have analyzed the biochemical characteristics of the proteins within the fraction containing the HCV particle and found a disulfide-bonded core protein complex (dbc-complex). We revealed that the disulfide-bonded dimer of core protein (dbd-core) was formed by a single cysteine residue at amino

* Corresponding author. Mailing address: Department of Viral Oncology, Institute for Virus Research, Kyoto University, 53 Kawahara-cho Shougoin, Kyoto 606-8507, Japan. Phone: 81-75-751-4046. Fax: 81-75-751-3998. E-mail: mhijikat@virus.kyoto-u.ac.jp.

† Supplemental material for this article may be found at http://jvi.asm.org/.

▽ Published ahead of print on 30 June 2010.

acid position 128 on the ER. The roles of the disulfide bond of the core protein in virus-like particle formation are discussed in this paper.

MATERIALS AND METHODS

Cell culture. Cells of the HuH-7 and HuH-7.5 human hepatoma cell lines were grown in Dulbecco's modified Eagle's medium (Nacalai Tesque, Kyoto, Japan) supplemented with 10% fetal bovine serum, 100 U/ml nonessential amino acids (Invitrogen, Carlsbad, CA), and 100 μg/ml each penicillin and streptomycin sulfate (Invitrogen).

Antibodies. The antibodies used for immunoblotting and indirect immunofluorescence analysis were specific for core protein (antibody 32-1), FLAG M2 (Sigma-Aldrich, St. Louis, MO), c-myc (Sigma-Aldrich), NS5A protein (CL1), adipocyte differentiation-related protein (ADRP; StressGen, Victoria, British, Columbia, Canada), calnexin (Calnexin-NT; StressGen), and glyceraldehyde-3-phosphate dehydrogenase (GAPDH; Chemicon, Temecula, CA). Antibodies specific for core protein (antibody 32-1) were a gift from M. Kohara (The Tokyo Metropolitan Institute of Medical Science, Tokyo, Japan). Rabbit polyclonal anti-NS5A protein CL1 antibodies have been described previously (36).

Plasmid construction. All plasmids were generated by inserting PCR-amplified fragments into expression plasmids. The plasmids, primer sequences, templates for the PCRs, and restriction enzyme sites used to construct the plasmids are listed in Table S1 in the supplemental material. Plasmids pJFH1^{E2FL} (encoding the full-length HCV genome with the FLAG epitope in the E2 hypervariable region), pJFH1^{AAA99} (encoding a NS5A mutant of JFH1^{E2FL}, resulting in noninfectious HCV particles), pJFH1$^{PP/AA}$ (encoding a core protein mutant of JFH1^{E2FL}, which allows replication in cells but prevents HCV particle production), and pcDNA3-core^{WT} (an expression plasmid encoding the full-length core protein of JFH1) have been described previously (36). Plasmid pJ6/JFH1, which contains the full-length HCV genome encoding structural proteins from the J6 strain and nonstructural proteins from the JFH1 strain, was kindly provided by Charles M. Rice (The Rockefeller University, New York, NY).

***In vitro* transcription.** RNA for transfection was synthesized as described previously (36). In brief, plasmids carrying the HCV RNA sequence were linearized with XbaI and used as templates for *in vitro* transcription with MEGAscript T7 (Ambion, Austin, TX).

Transfection. Ten micrograms of JFH1^{E2FL}, JFH1^{C128A}, JFH1^{C184A}, JFH1$^{C128/184A}$, JFH1$^{PP/AA}$, or JFH^{AAA99} and J6/JFH1 or J6/JFH1^{AAA99} RNAs were transfected into HuH-7 and HuH-7.5 cells (1.0×10^7 cells) by electroporation (260 V, 0.95 μF) using a Gene Pulser II system (Bio-Rad, Hercules, CA). Core protein expression plasmids were transfected into HuH-7 cells using Lipofectamine LTX (Invitrogen), according to the manufacturer's protocol.

HCV particle precipitation. Culture medium from HCV RNA-transfected cells were concentrated using Amicon Ultra-15 centrifugal filters with Ultracell-100 membranes (Millipore, Billerica, MA) and mixed with sucrose solution in phosphate-buffered saline (PBS) to a final sucrose concentration of 2%. This mixture was ultracentrifuged (100,000 × *g*, 4°C for 2 h), and the HCV particles were obtained as a pellet. The pellet was then suspended in culture medium for infection experiments or PBS for immunoblot analysis.

Indirect immunofluorescence analysis. Indirect immunofluorescence analyses of HCV infection and the cellular localization of the HCV proteins were performed as described previously (36).

Protease protection assay. Concentrated culture medium from JFH1^{E2FL} RNA-transfected HuH-7 cells was fractionated using 20 to 50% sucrose density gradients, and the HCV RNA titer was measured in quantitative reverse transcription-PCRs (RT-PCRs) as described below. Fractions with high HCV RNA titers were collected, and JFH1^{E2FL} particles were obtained as a pellet after ultracentrifugation (100,000 × *g*, 4°C for 2 h). The pellet was suspended in PBS and treated with 10 μg/ml trypsin or 5 μg/ml proteinase K in the presence or absence of 1% Nonidet P-40 (NP-40) at 37°C for 15 min, unless otherwise indicated. The reaction was quenched by the addition of protease inhibitor cocktail (Nacalai Tesque), followed by SDS-PAGE under nonreducing conditions and immunoblotting specific for core protein.

Immunoblot analysis. Samples were subjected to SDS-PAGE in sample buffer (62.5 mM Tris-HCl [pH 7.8], 1% SDS, 10% glycerol) with or without 5% β-mercaptoethanol (β-ME) or 50 mM dithiothreitol (DTT) for reducing and nonreducing conditions, respectively. *N*-Ethylmaleimide (NEM; Nacalai Tesque) was added to the sample buffer to a final concentration of 5 mM for the indicated samples. Proteins were transferred to a polyvinylidene difluoride membrane and blocked in blocking buffer for 1 h at room temperature with gentle agitation. After incubation with primary antibodies overnight at 4°C, the membrane was washed three times for 5 min in washing buffer at room temperature with gentle agitation. The membrane was then incubated with horseradish peroxidase (HRP)-conjugated secondary antibodies for 1 h at room temperature. After three washes in washing buffer, proteins were detected using Western Lightning reagent (PerkinElmer, Waltham, MA) or ECL Advance (GE Healthcare, Buckinghamshire, England) and Kodak MXJB Plus medical X-ray film (Kodak, Rochester, NY) or an LAS-4000 system (Fujifilm, Tokyo, Japan).

Preparation of LDs. LDs were prepared as described previously (36).

Preparation of MMFs. Microsomal membrane fractions (MMFs) were collected as described previously (15) with some modifications. In brief, cells were collected in homogenization buffer (20 mM Tris-HCl [pH 7.8], 250 mM sucrose, and 0.1% ethanol supplemented with protease inhibitor cocktail) and homogenized on ice using 40 strokes of a Dounce homogenizer. The samples were then centrifuged at 1,000 × *g* for 10 min at 4°C. The supernatant was collected in a new tube and centrifuged again at 16,000 × *g* for 20 min at 4°C. The supernatant was further centrifuged at 100,000 × *g* for 1 h at 4°C. The MMF precipitate was homogenized in lysis buffer (1% NP-40, 0.1% SDS, 20 mM Tris-HCl [pH 8.0], 150 mM NaCl, 1 mM EDTA, and 10% glycerol supplemented with protease inhibitor cocktail) using a Dounce homogenizer.

qRT-PCR analysis. Quantitative RT-PCR (qRT-PCR) analysis for determination of the HCV RNA titer was performed as described previously (36).

ELISA specific for core protein. The core protein in culture medium was quantified using an enzyme-linked immunosorbent assay (ELISA; HCV antigen ELISA; Ortho-Clinical Diagnostics, Raritan, NJ), according to the manufacturer's protocol.

RNA-protein binding precipitation assay. Core^{WT} or core^{C128A} was translated *in vitro* from pcDNA3-core^{WT} and pcDNA3-core^{C128A}, respectively, using a TNT-coupled rabbit reticulocyte lysate system (Promega, Madison, WI), according to the manufacturer's protocol. These proteins were incubated with poly(U) agarose (Sigma) in binding buffer (50 mM HEPES (pH 7.4)–100 mM NaCl–0.1% NP-40–20 U RNase inhibitor) at 4°C for 2 h with or without RNase A. After five washes, the resin-bound core proteins were immunoblotted.

RESULTS

The HCV particle contains core protein complex formed by a disulfide bond. To analyze the core protein of the HCV particle, we first subjected the concentrated culture medium of HuH-7 cells transfected with *in vitro*-transcribed JFH1^{E2FL} RNA to ultracentrifugation. After the resulting pellet was resuspended in culture medium, we confirmed the presence of infectious HCV particles on the basis of the infectivity of HuH-7.5 cells (Fig. 1a). The infectious JFH1^{E2FL} particle-containing pellet was separated by SDS-PAGE under nonreducing conditions, and immunoblot analysis showed the presence of a core antibody-reactive protein that was approximately twice the size of the core protein (38 kDa), in addition to the expected 19-kDa core protein (Fig. 1b, lane 1). Because treatment with DTT eliminated the larger core protein antibody-reactive band while the levels of the core protein monomer increased (Fig. 1b, lanes 2 to 6), the larger protein likely represented a dbc-complex. This complex was also found in J6/JFH1-derived particles (see Fig. S2 in the supplemental material), indicating that the complex was not specific for JFH1^{E2FL}.

To determine whether the dbc-complex is a component of the HCV particle, a protease protection assay was performed using RNase-resistant HCV particles fractionated on the basis of their buoyant densities. Concentrated culture medium from HuH-7 cells transfected with *in vitro*-transcribed JFH1^{E2FL} RNA was fractionated using a 20 to 50% sucrose density gradient; and JFH1^{E2FL} particles, which were presumed to contain both infectious and noninfectious particles, were collected from fractions with high HCV RNA titers using ultracentrifugation (Fig. 2a, fractions 8 to 13). The core protein from the collected fractions was analyzed by immunoblotting after SDS-

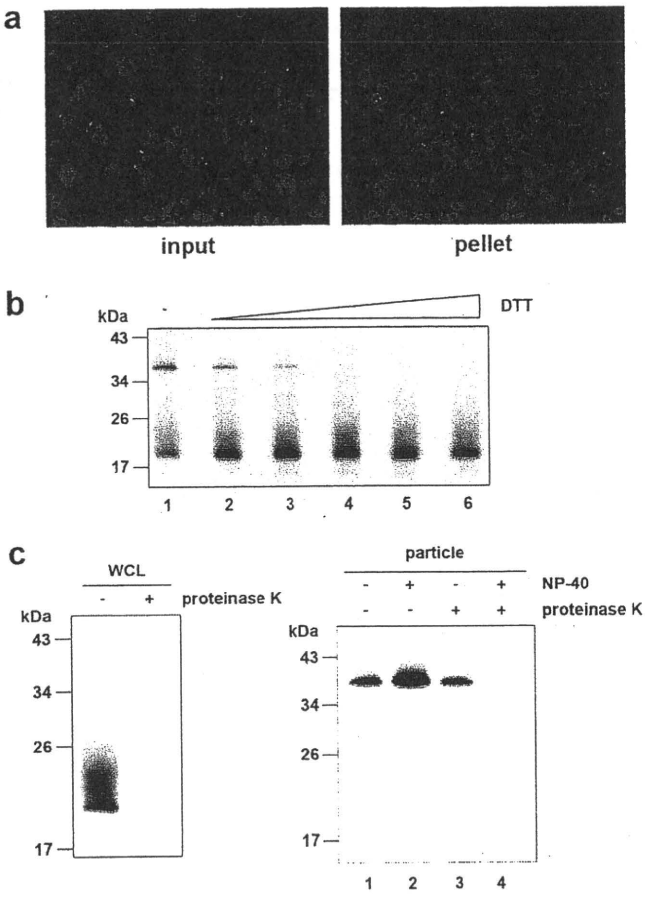

FIG. 1. The HCV-like particle consists of a core complex formed by a disulfide bond. (a) The infectivity of the pellet fraction collected from concentrated culture medium from JFH1^{E2FL} RNA-transfected HuH-7 cells was analyzed as described in Materials and Methods. Input indicates the same volume of concentrated culture medium used to pellet the virus-like particles. (b) Immunoblot analysis of the core protein in pellets containing JFH1^{E2FL} virus particles treated with various levels of DTT (lanes 1, 2, 3, 4, 5, and 6, 0, 1.56, 3.13, 6.25, 12.5, and 25 mM DTT, respectively). (c) Immunoblot analysis of the core protein in JFH1^{E2FL} particles collected from sucrose density gradient fractions with high HCV RNA titers (particle) (Fig. 2a, fractions 8 to 13) and treated with 5 μg/ml proteinase K at 37°C for 15 min in the presence or absence of 1% NP-40 (right panel). As a positive control, WCL prepared from JFH1^{E2FL} RNA-transfected HuH-7 cells in lysis buffer was treated with 5 μg/ml proteinase K at 37°C for 15 min (left panel). Data are representative of three independent experiments.

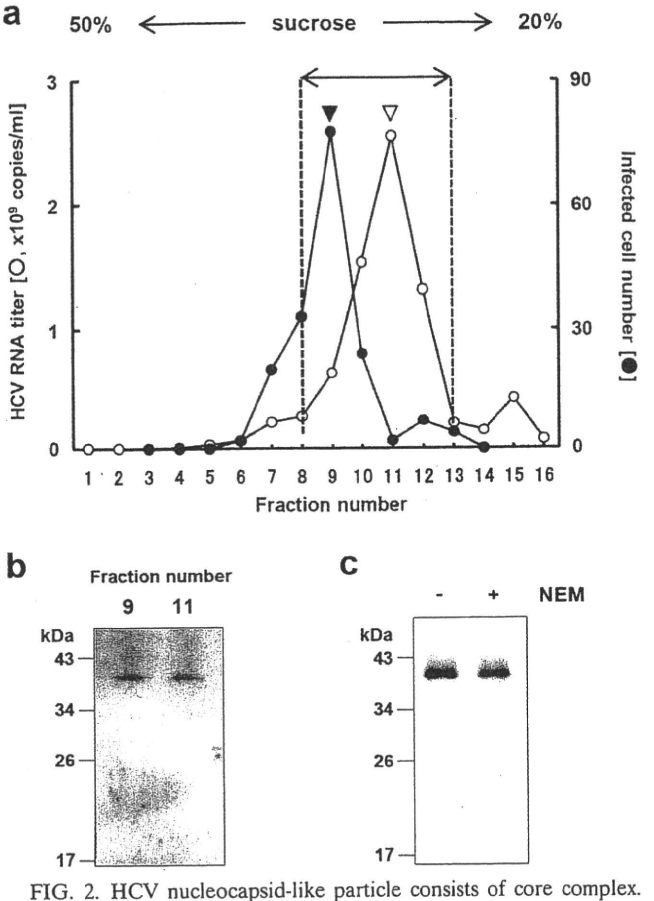

FIG. 2. HCV nucleocapsid-like particle consists of core complex. (a) HCV RNA titer in culture medium separated on a 20 to 50% sucrose density gradient. Concentrated culture medium from JFH1^{E2FL} RNA-transfected HuH-7 cells were treated with RNase and separated on a 20 to 50% sucrose density gradient. Fractions 1 to 16 were obtained from the bottom to the top of the tube, respectively. The HCV RNA titer and infectivity of each fraction were analyzed by real-time qRT-PCR (for fractions 1 to 16) and counting the number of cells infected with HCV-like particle detected by immunofluorescence (for fractions 3 to 14), respectively, as described in Materials and Methods. In brief, each fraction was diluted with 1× PBS and HCV-like particles were collected by ultracentrifugation, and then the pellets were suspended in culture medium and used for infection. (b) HCV-like particle collected from the infectious HCV peak (from panel a, filled arrowhead) and the HCV RNA peak (from panel a, open arrowhead) were collected by ultracentrifugation, subjected to nonreducing SDS-PAGE, and detected by immunoblotting against the core protein. (c) HCV-like particles collected from fractions 8 to 13 (a) were subjected to nonreducing SDS-PAGE in the presence (lane +) or absence (lane −) of 5 mM NEM and analyzed by immunoblotting against the core protein. Data are representative of two (a, infectivity of fractions) or three independent experiments.

PAGE under nonreducing conditions and showed only the dbc-complex (Fig. 1c, right panel).

To examine whether the complex contributes to the infectivity of the particles, we analyzed the dbc-complex in the fractions containing infectious and noninfectious HCV particles (fractions 9 and 11 of Fig. 2a, filled and open arrowheads, respectively). Both the infectious and noninfectious HCV particle-containing fractions contained the dbc-complex (Fig. 2b). To confirm this further, a pellet containing particles of mutant JFH1^{AAA99}—a mutant of JFH1^{E2FL} that primarily produces noninfectious particles (36)—was analyzed in a similar manner. These dbc-complexes were found in pelleted particles of both JFH1^{AAA99} and J6/JFH1^{AAA99}, which was a mutant J6/JFH1 with a similar substitution to JFH1^{AAA99} (see Fig. S2 in the supplemental material). These results indicated that the dbc-complex was present in both the infectious and noninfectious HCV-like particles.

The core protein monomer observed in the pellet samples (Fig. 1b) may be from the secreted core protein or the debris of apoptotic cells, because the core protein is known to be secreted from cells expressing this protein under particular conditions (42) and strain JFH1 is known to cause apoptosis (45). The dbc-complex-specific signals in the HCV particles seem to be increased in the NP-40-treated samples for some

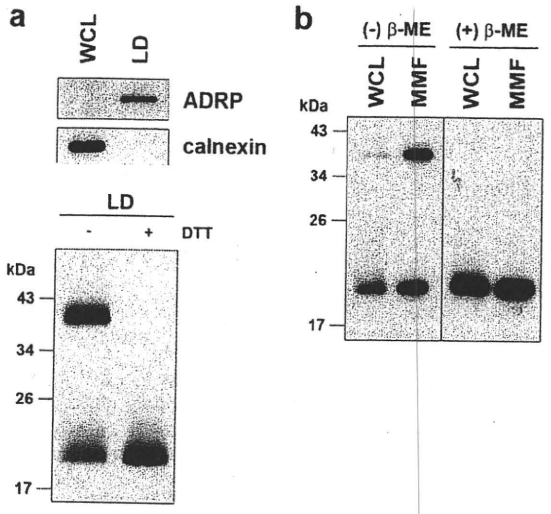

FIG. 3. The core complex is formed at the LD and ER. (a) The LD fraction and WCL were collected from JFH1^{E2FL} RNA-transfected HuH-7 cells on day 5 posttransfection. (upper panel) Immunoblot analysis of the LD marker ADRP and the ER marker calnexin in the LD fraction; (lower panel) immunoblot analysis of the core protein in the LD fraction treated or not treated with 50 mM DTT. (b) Immunoblot analysis of the core protein in the MMF and WCL collected from JFH1^{E2FL}-producing HuH-7 cells on day 5 posttransfection in the presence or absence of 5% β-ME. Data are representative of those from three independent experiments.

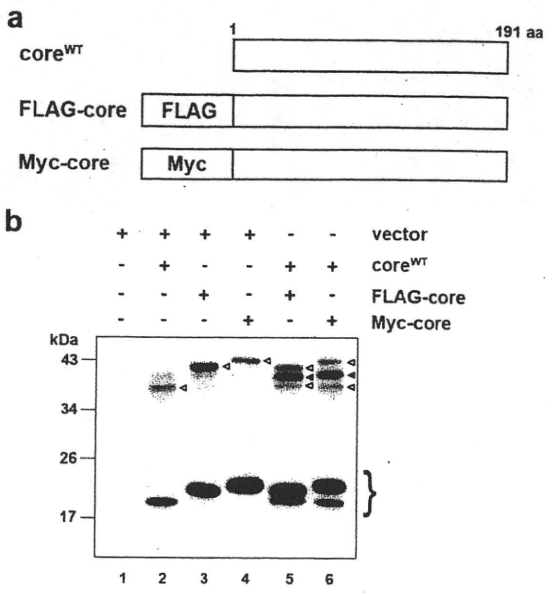

FIG. 4. The core complex consists of a core dimer. (a) Schematic of wild-type, FLAG-tagged (FLAG-core), and Myc-tagged (Myc-core) core proteins. (b) Immunoblot analysis of the core protein in the MMF collected from HuH-7 cells transfected with combinations of pcDNA3 (vector) and/or core expression plasmids (e.g., encoding core^{WT}, FLAG-core, and Myc-core), as indicated. The experiment was performed under nonreducing conditions. The lower bands represent core monomer (marked on the right with a brace). White arrowheads, bands corresponding to dbd-core; black arrowheads, positions of the intermediately sized core complex formed by core^{WT} and the tagged core. Data are representative of those from three independent experiments.

unknown reason (Fig. 1c, lanes 1 and 2). Although the intermolecular disulfide bond is known to be artificially formed in denaturing SDS-PAGE in the absence of reducing agents, the dbc-complex was still observed even in the presence of NEM, which is the alkylating agent for free sulfhydryls, during sample preparation (Fig. 2c), indicating that the dbc-complex was naturally present in the virus-like particles.

The HCV nucleocapsid is covered with lipid membranes and E1 and E2 proteins, making it resistant to proteases. As expected, in the absence of NP-40, the dbc-complex was resistant to proteinase K (Fig. 1c, lane 3), whereas proteinase K was able to digest core protein in whole-cell lysates (WCLs) collected from JFH1^{E2FL}-transfected HuH-7 cells (Fig. 1c, left panel). Disrupting the envelope structure with NP-40 made the dbc-complex susceptible to proteinase K treatment (Fig. 1c, lane 4), indicating that the dbc-complex was indeed a component of the HCV particle.

The dbc-complex forms on the ER. To investigate the subcellular site at which the dbc-complex forms, LDs and MMFs from JFH1^{E2FL} replicating HuH-7 cells were analyzed by immunoblotting. We first analyzed the dbc-complex in LDs, because LDs are involved in infectious HCV particle formation (36, 47). The purity of the LD fraction was determined using immunoblot analysis of calnexin and ADRP, ER and LD marker proteins, respectively (Fig. 3a, upper panel). The core protein was then analyzed in the LD fraction. As shown in Fig. 3a (lower panel), the dbc-complex was observed in the LD fraction from JFH1^{E2FL} RNA-transfected HuH-7 cells. We next analyzed the core protein in the ER-containing MMF, because the core protein is first translated and processed on the ER (16). As shown in Fig. 3b, the dbc-complex was observed in the MMF from JFH1^{E2FL} RNA-transfected HuH-7 cells. These results suggest that the dbc-complex is first formed at the ER. To assess the possibility that dbc-complex-containing HCV particles were also assembled on the ER, the sensitivity of the dbc-complex to protease treatment was analyzed. The dbc-complex in the MMF was susceptible to protease treatment in the absence of NP-40, indicating that the dbc-complex on the ER was not yet part of a HCV particle (data not shown).

dbc-complex is most likely a disulfide-bonded dimer form of the core. In order to examine whether the core protein itself has the potential to form a dbc-complex, we analyzed the dbc-complex formation of the full-length wild-type core protein (core^{WT}) expressed from pcDNA3-core^{WT} (36), the expression plasmid encoding the 191-amino-acid full-length core protein of JFH1 strain. We used this expression plasmid because the core protein from this plasmid was likely to be processed correctly enough to produce infectious HCV particles when it was cotransfected with the RNA of JFH1^{dc3}, which is a core protein deletion mutant of JFH1 (36). As a result, the dbc-complex formation was observed from the MMF of core^{WT}-expressing cells both in the absence and in the presence of NEM (Fig. 4b; lane 2 and data not shown, respectively). We next investigated the effect of the amino acid region of E1 on the production of the dbc-complex, because it has been reported that the efficient processing of core protein is dependent on the presence of some E1 sequence to ensure the insertion of the signal sequence for E1 in the translocon/membrane machinery (34). The dbc-complex was also observed